AN ABSTRACT OF THE THESIS OF

Thomas W. Eichenberg, Jr. for the degree of Master of Science in Nuclear Engineering presented on August 21, 1990.

Title: Numerical Analysis of Condensation Induced Water-Hammer in Horizontal Piping Systems

Abstract approved: Redacted for Privacy
Dr. Jose N. Reyes

Condensation Induced Water-Hammer, CIWH, has been an historical problem for the nuclear power industry over the past 2 decades. It has caused damage to plant systems, and considerable anguish to plant operators. This thesis has embarked on an attempt to characterize the fluid motion, heat transfer, mixing, and stability of a horizontal, stratified flow of steam over subcooled water.

A literature review was conducted to determine the state of numerical and analytical methods which have been applied to this problem. The result of the review has led to the implementation of new analytical interfacial stability models. Information from the review has also led to the development of correlations for wave frequency and amplitude on the phase interface.

A numerical model has been developed to estimate the temperature profile on the phase interface. Also, the model will construct, by use of the above correlations, an estimate of the interface wave structure. This wave structure is then evaluated against a non-linear model for interface stability to determine the onset of slug formation.

The numerical model has been used to evaluate two known CIWH events. The results indicate that the onset of slug formation is necessary, but not sufficient, to ensure a water-hammer event. The results imply that there is the possibility that once a slug has formed, it may break up before a trapped steam void can fully collapse. The model also indicates that CIWH in steam generator, feedwater nozzle sections is not due to the formation of slug on an unstable phase interface. Rather, CIWH may occur when the liquid level inside of the feedwater nozzle is above the top of the feedring, thus creating an isolated steam pocket. The rapid condensation of the trapped steam in the causes CIWH. This particular result implies that it may be possible to completely avoid CIWH in the feedwater nozzle altogether.

NUMERICAL ANALYSIS OF CONDENSATION INDUCED WATER-HAMMER IN HORIZONTAL PIPING SYSTEMS

by

Thomas William Eichenberg, Jr.

A THESIS

submitted to

Oregon State University

in partial fulfillment of
the requirements for the
degree of

Master of Science

Completed August 21, 1990

Commencement June 1991

APPROVED:

Redacted for Privacy

Professor of Nuclear Engineering in charge of major

Redacted for Privacy

Head of department of Nuclear Engineering

Redacted for Privacy

Dean of Graduate School

Date thesis is presented August 21, 1990

Typed by: Thomas William Eichenberg, Jr.

Acknowledgement

I would like to thank my major professor, Dr. J.N. Reyes, for his help in wadding through the multitude of topics covered by this thesis. I would also like to thank Mr. Ajay Anand for his patient listening when I would ramble through some of my theories. Finally, I would like to thank Portland General Electric Company, (PGE), for supporting my research under contract P.O. N-55576; your help has been greatly appreciated.

Table of Contents

Numerical Analysis of Condensation Induced Water-Hammer in Horizontal Piping Systems

List of Figures

Numerical Analysis of Condensation Induced Water-Hammer in Horizontal Piping Systems

1. INTRODUCTION

The thermal-hydraulic phenomenon of condensation induced water-hammer, (CIWH), is of particular interest to the commercial nuclear power industry. Probably the most important reason for this interest stems from the potential for serious damage to both primary and secondary piping systems. The possible piping systems damage can range from a purely elastic deformation of pipe components to a large break, loss of coolant accident, (LOCA). It is the possibility of the large break LOCA, or a rupture of main steam lines that has implications for plant integrity and public safety.

For the nuclear plant systems designer, the interest in CIWH takes on a greater economic light. The system designer who can achieve design requirements, while avoiding the geometries associated with CIWH, can also avoid the possible need for replacement of damaged systems. Likewise, from the plant operators' perspective, knowing the limits of operating parameters for unavoidable CIWH geometries makes it possible to avoid plant damage and the resulting loss of plant availability.

1.1 TYPE

There are different types of CIWH. The differences are primarily the result of the geometry. However, all CIWH events share a common mechanism: a steam void is cut off from its steam supply which results in void collapse. Figure 1, Figure 2, Figure 3, & Figure 4 represent a time line for pipe filling, water slug formation, acceleration, and finally, slug impact and pressure wave formation.

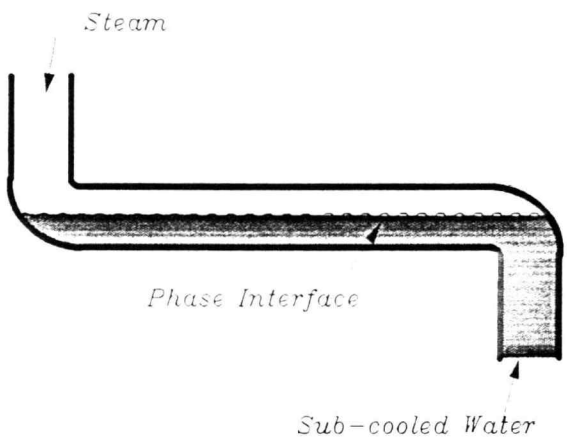

Figure (1): Pipe Refill

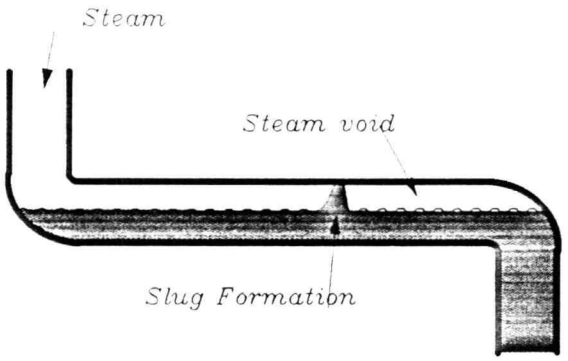

Figure (2): Bridging

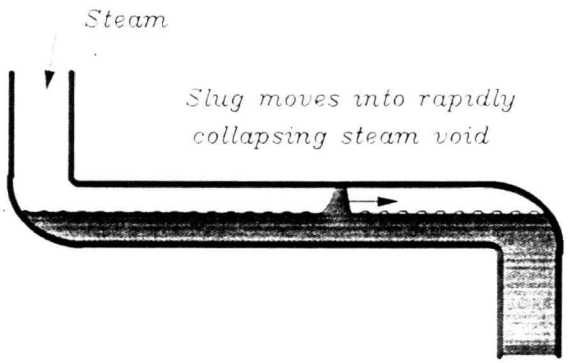

Figure (3): Slug Acceleration

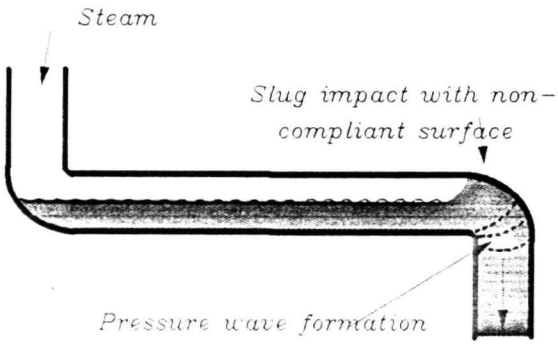

Figure (4): Slug Impact

This thesis, as indicated by the title, will concentrate only upon void collapse in horizontal piping systems as indicated in the above sequence of pictures. In particular,

the two specific cases to be looked at involve the main feedwater line to top-feed steam generators of pressurized water reactors, (PWR's). The cases to be analyzed involve sub-cooled water refilling a steam voided line.

The main feedwater line to the steam generator generally has two horizontal sections at different elevations. The highest horizontal section is located at the hookup to the steam generator nozzle. This high section is usually 1-5 meters in length and 25-45 centimeters in diameter. The lower horizontal section, the main feedline, can be over 50 meters long with multiple bends and essentially the same diameter as the high elevation section.

1.2 MODE OF ISOLATION

Figure 5 shows the high horizontal section at the penetration to the steam generator. The mode of steam void isolation is the result of slug formation, also known as "Bridging". Bridging is the result of a thermal-hydraulic instability at the wavy phase interface between the steam and sub-cooled water.

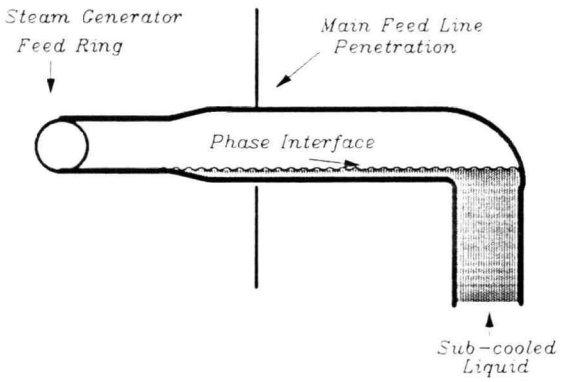

Figure (5): Steam Generator Penetration

The interfacial instability is a complicated function of geometry, fluid properties, interface wave structure, and relative motion between the two fluid phases. Under certain conditions, the wave structure can become unstable, with a rapid amplification of wave amplitude. This can lead to isolation of the steam void as shown in Figure 2.

1.3 GENERATION OF UNSTABLE CONDITIONS

Geometry is only part of the cause for CIWH. As mentioned above, relative motion between the two fluid phases is very important, and this is where the condensation process is involved. In fact, the dynamic behavior of the system is closely coupled to the condensation heat transfer process. Figure 6 shows a simplified view of a horizontal section of pipe. Initially the pipe was completely filled with steam. Hence, the only heat transfer mechanism at work is the condensation on the inside pipe wall. Therefore, the initial velocity profile of the steam in the pipe section is due to condensation onto the pipe wall. Now, as the pipe begins to

refill with sub-cooled water, the interfacial surface area between the two phases allows for direct contact condensation to take place. Therefore, the axial velocity profile of the steam is a function of two different condensation processes.

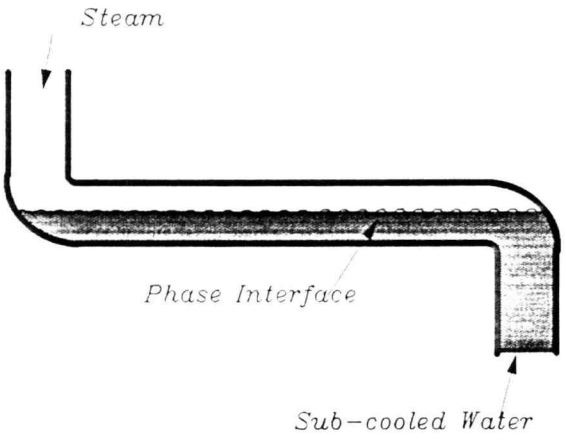

Figure (6): Interface Surface Area

Because the heat transfer mechanism is condensation, there is mass transfer from the vapor phase to the liquid phase. It is possible to think of the velocity profile for the steam as the result of a mass demand due to the condensation heat transfer. This mass demand generates a mass flow rate of steam as a function of time and space within the pipe, and the mass flow rates can be converted into a velocity profile as a function of time and space. The relative motion of the steam over the water, due to the mass demand, causes waves to form at the phase interface, effectively increasing the direct contact surface area. Consequently, the mass demand at the interface is increased which in turn generates greater relative motion between the two phases. The further

increase of relative motion creates a more highly agitated phase interface which leads to greater heat transfer which leads to more agitation and on and on and on. Over time, this would seem to spiral out of control.

There is, however, a breaking mechanism to this runaway process. The mass which is condensed from steam to water must mix with the sub-cooled liquid. This mixing of the condensate and water will increase the temperature of the liquid phase in the pipe. Hence, the magnitude of the temperature gradient, which drives the condensation process, is decreased. If the rate at which the temperature gradient falls is greater than the rate of increase in interfacial surface area, then the entire system will move toward a more stable process. For those who are familiar with nuclear reactor physics, the mixing process acts much like that of negative temperature coefficients of reactivity in fuel rods where the reaction cross-sections are reduced with increasing temperature.

1.4 OBJECTIVES

The primary objective of this thesis is to make a numerical estimate of the transient condensation behavior for a horizontal pipe refill scenario. A major goal of the estimate will be to determine conditions which could lead to the onset of bridging. Additional goals include, estimates of the system over-pressure and forces which non-compliant surfaces

in the pipe system could be subjected. (Non-compliant surfaces are those surfaces which would bear the direct impact of an accelerated water slug. They include elbows, side walls in T-fittings, valves, and pumps.)

2 REVIEW OF THE LITERATURE

The nature of the CIWH problem is so complex that the literature review must cover a wide range of topics. The pressure drop within the pipe due to interfacial shear stress cannot be modelled using friction factors developed for smooth pipes. Likewise the condensation heat transfer coefficients for the interface can not be modelled using a simple Dittus-Boelter correlation. Also, as will be discussed below, there are many different methods for determining the onset of slug formation. Hence, the major topics of the review include flow pattern mapping, slug formation, interfacial shear stress, (pressure drop), and heat transfer.

2.1 HISTORY OF CIWH

CIWH has primarily been a problem associated with the commercial nuclear power industry. The following list of publications from the Nuclear Regulatory Commission, (NRC), provides an extensive evaluation of the industrial experience with CIWH:

NUREG-0291
NUREG-0582
NUREG-0993
NUREG-0927
NUREG/CR-1606
NUREG/CR-2059
NUREG/CR-3939

There were over 200 CIWH events reported to the NRC between 1969 and 1986. NUREG/CR-5220 is the NRC manual for inspectors dealing with the topic of CIWH, and discusses methods of analysis as well as specific case studies of past CIWH occurrences. This thesis will make use of the NRC methods and attempt to replicate some of the case studies.

2.2 FLOW REGIME MAPS

Flow regime maps represent the earliest method for predicting the hydraulic behavior of a two-phase system. With respect to CIWH, flow regime maps have been used to predict the onset of a slug flow pattern. The merits of using flow regime maps for prediction of bridging will be discussed in section 2.2.1, 2.2.2, and 2.2.3

A flow map may be described in general as being a 2-dimensional view of a parameter field. That is to say, for two different parameters on two separate axes, usually dimensionless, boundary curves are drawn which separate the map into distinct zones. Each zone representing a particular hydraulic flow behavior. Figure 7 shows a generic example of flow regime map.

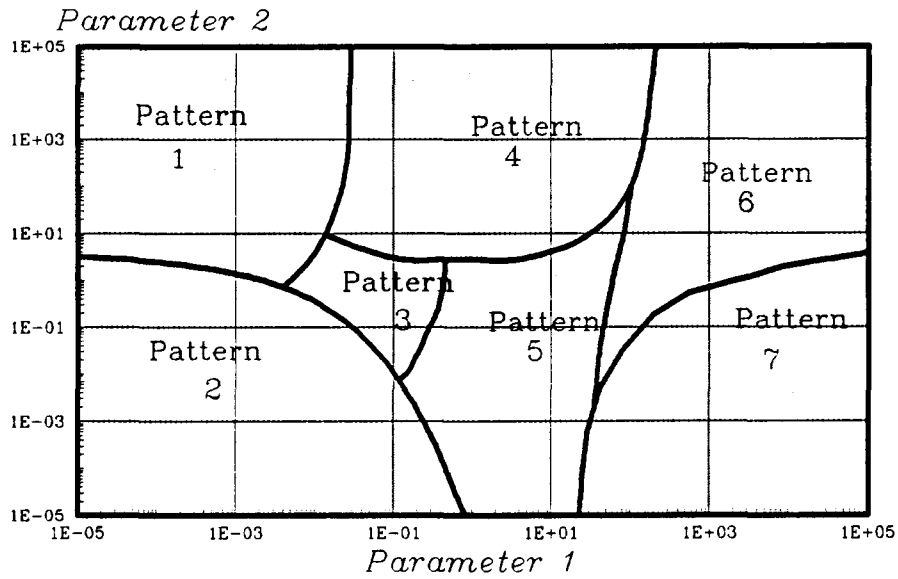

Figure (7): Flow Regime Map

A flow regime map has a large range and domain of application. These range and domain values typically cover many orders of magnitude. Because of the large range and domain, many different flow patterns can be included on the map. Some common flow patterns include bubbly, plug, stratified, wavy, slug, annular, and spray or mist.

The first important flow map to be published was by Ovid Baker, [1], in 1954. His flow map was developed for the flow of oil and natural gas in the same pipeline. The results of Baker's map were then applied to the design of multiphase pipelines for oil and natural gas.

The development and use of flow maps remained within the scope of chemical engineering, particularly in crude oil applications, up to the early 1970's. During this time

period, the application of flow maps expanded to include pressure drop, and liquid holdup estimation. Papers by S.S. Agrawal, G.A. Gregory, & G.W. Govier, [2], and J.M. Mandhane, G.A. Gregory, & K. Aziz, [3], provided substantial improvement and verification of the original work by Baker. Specifically, the new works of Agrawal, and Mandhane introduced the use of dimensionless groups of physical properties as flow map axis parameters.

Papers by P.L. Spedding & Van Thanh Nguyen, [4], and Yoshihiro IIDA, [5], during the mid and late 1970's, brought forward flow regime maps for general gas-liquid flows. Although these new maps were the result of air-water experiments, they were generally considered acceptable for use with any fluid component arrangement.

The early 1980's saw papers by Dvora Barnea, Ovadia Shoham, Yehuda Taitel, & A.E. Dukler, [6], and Ovadia Shoham & Yehuda Taitel, [7], which were concerned with the geometry dependence of flow pattern maps. In particular a distinction was being drawn between flow pattern maps for vertical or horizontal and inclined flow. However, almost as soon as flow maps were becoming differentiated by geometry, a paper by Dvora Barnea, [8], proposed a unified model for all inclination angles!

It was not until recently that a paper by T.N. Tandon, H.K. Varma, & C.P. Gupta, [9], became concerned with the problem of mass transfer between fluid phases. Even more

recently, papers by A. Matuszkiewicz, J.C. Flamand, & J.A. Boure, [10], and P.Y. Lin & T.J. Hanratty, [11], and N. Andritsos & T.J. Hanratty, [12], have shown an interest in flow transition between specific patterns as well as the instabilities which produce the pattern changes.

2.2.1 COMMENTS

The concept of flow pattern maps and their subsequent application are of immediate concern to the systems designer. Flow pattern maps have advantages and disadvantages associated with them depending upon the problem to which they are applied.

2.2.2 ADVANTAGES

Flow pattern maps have a distinct advantage due to their ease of use. This stems from the fairly simple parameters, (not true for all maps), which are used as axis values on the map. Using these maps allows for fast estimation of the flow pattern to be encountered. This in turn makes it a straight forward matter to estimate pressure losses and thus simple to estimate required piping and pump requirements.

2.2.3 DISADVANTAGES

Flow pattern maps also have some sharp disadvantages. The most prominent of these is the subjective nature of flow pattern definitions. What one person considers to be the transition from one pattern to another may be

different from the opinion of a second or third party. At the same time, everyone could be in agreement on the pattern transition but have a different name for the different pattern, leading to confusion in the interpretation of the data. Also, for some types of fluids, flow patterns may or may not even be defined with respect to another fluid. As an example, it is not clear that highly viscous fluids possess flow patterns identical to nearly inviscid or even Non-Newtonian fluids.

A second area of concern is the lack of a strong theoretical base for these flow maps. These maps are, for the most part, empirical results. The absence of a strong theoretical basis for flow maps should be cause for hesitation in applying a flow map to designs which are significantly different than the experiments conducted to generate the map data base.

2.3 SLUG FORMATION

Because this thesis is concerned with the actual onset of bridging, and because of the need for a stronger theoretical basis to predict the phenomenon, it is necessary to look at papers which are specifically concerned with the onset of bridging. The first qualitative and quantitative discussion came from H. Helmholtz, **[13]**, in 1868, and Lord Kelvin, **[14]**, in 1910. The theory of interface instability has since been known as Kelvin-Helmholtz instability theory. A complete

discussion of Kelvin-Helmholtz theory can be found in a book by S. Chandrasekhar, [15]. The many different theories which are available to describe the onset of bridging can basically be divided into two groups. Those which are based on Kelvin-Helmholtz instability theory, and those which are not.

2.3.1 KELVIN-HELMHOLTZ BASED

The first Kelvin-Helmholtz based theory on bridging in horizontal piping systems was presented by E.S. Kordyban & T. Ranov, [16], in 1970. This paper suggested that the onset of bridging could be predicted using a linear Kelvin-Helmholtz model. Additional papers by Y. Taitel & A.E. Dukler, [17], and K. Mishima & M. Ishii, [18], and E. Hihara & T. Saito, [19], and P.Y. Lin & T.J. Hanratty, [20], made further refinements to the linear theory with new assumptions or by adding coefficients developed to correlate experimental data.

The first paper to present a nonlinear Kelvin-Helmholtz model of the onset of bridging was given by R. Ahmed & S. Banerjee, [21]. This paper used a perturbation method to get a third order approximation to the governing equation of fluid flow. The nonlinear model is capable of closely approximating the conditions which were drastically over estimated by the linear theory.

2.3.2 NON-KELVIN-HELMHOLTZ MODELS

The non-Kelvin-Helmholtz models are generally semi-empirical in nature employing experimental correlations to fit the model results to the experimental data. The first paper to use this approach was presented by G.B. Wallis & J.E. Dobson, [22]. This paper makes assumptions about the wave structure of the interface which take it out of the purely Kelvin-Helmholtz theory. Wallis and Dobson then proceed to relate the stability of the assumed surface structure to the superficial velocity of the two fluids. This paper is important because the experiments which are outlined were the first to show that the linear Kelvin-Helmholtz models are inadequate for predicting the onset of bridging. Since the papers publication, the experimental results have become a benchmark for comparison of new theoretical models.

Recent papers by G.C. Gardner, [23], and J. Kubie, [24], and A.J. Johnston, [25], and W.P. Jepson, [26], have been presented which further attack the adequacy of linear Kelvin-Helmholtz theory to predict the onset of bridging because of the inaccuracy with experimental results. These papers made improvements to the Wallis and Dobson model and also presented new experimental data confirming the Wallis and Dobson data. Ultimately though, these papers became a digression to supporting the use of flow regime

maps for predicting the presence of slug flow.

2.3.3 COMMENTS

The centerpiece of this thesis is the incorporation of the nonlinear Kelvin-Helmholtz theory presented by Ahmed & Banerjee. This method has the strongest theoretical background. It also has the advantage of being capable of predicting the onset of bridging more accurately than the linear Kelvin-Helmholtz models.

2.4 INTERFACIAL SHEAR STRESS

Because the problem of CIWH involves the relative motion of two different phases past each other, there will undoubtedly be a shear stress at the interface boundary. The interfacial friction resulting from the shear stress will directly effect the pressure loss. Hence the physical properties of the steam will be changing with respect to position in the piping system. The variable nature of the steam properties will create variability in the heat transfer and subsequently, the velocity profile will have some dependence upon the magnitude of the shear stress. It is, therefore, important to be able to model the pressure losses in an accurate manner.

2.4.1 PRESSURE DROP

In 1949, R.W. Lockhart & R.C. Martinelli, [27], proposed a correlation for the pressure drop and liquid holdup of isothermal, two-phase flow. Virtually every paper on the subject prior to 1980 is either a direct descendant or an

improvement using new data. It is not until 1981, that a paper by the well known two-phase flow expert V. Kadambi, [28], begins to deal with the problem of pressure drop for a specific flow regime. Yet, even at that point in time, the theoretical development is heavily influenced by the methods used in flow pattern map analysis as well as the method of Lockhart and Martinelli.

It is only within the last decade that theoretical and experimental investigation has focused attention on pressure drop in specific flow patterns. This focus has been upon the strong development of theoretical forms for the interfacial shear stress in tandem with trying to experimentally measure the interfacial shear stress. Papers by A.J. Johnston, [29], and Y.L. Sinai, [30], and N. Andritsos & T.J. Hanratty, [31], and Y. Hagiwara, E. Esmaeilzadeh, H. Tsutsui, & K. Suzuki, [32], and J. Hart, P.J. Hamersma, & J.M.H. Fortuin, [33], show that the new semi-theoretical models are a good match to the newly measured data on interfacial shear stress.

From the stand point of applicability to the specific CIWH problems of this thesis, none of the above mentioned methods of estimating the interfacial shear stress are satisfactory. The primary reason for this is the stagnant nature of the sub-cooled liquid phase. In this thesis, the sub-cooled liquid has no bulk velocity in the axial

direction of the pipe. Hence, the liquid phase Reynolds number is zero. Therefore, any friction factor correlation which requires the use of the liquid phase Reynolds number can not be satisfied. There is however, a correlation presented by H.J. Kim, [34], which can produce an estimate of the interfacial shear stress even when the Reynold number goes to zero. This method will be discussed in more detail in the chapter on methods.

2.5 HEAT TRANSFER

The mode of heat transfer which is important to the problem of CIWH is condensation. For the particular problem to be addressed in this thesis, both direct contact, and filmwise condensation processes are involved. Therefore, the literature review in heat transfer will be confined to these two areas.

2.5.1 FILM CONDENSATION

For the most part, condensation processes in industry are conducted on the external side of tubes. That is to say, on the shell side of a heat exchanger. The first person to look at this method of heat transfer was Nusselt, [35], in 1916. The results of Nusselt's analysis have remained at the center of condensation heat transfer theory to this day. The first major attempt to look at tube side condensation came from D. Butterworth, [36], in 1974. As Dr. Butterworth noted in his paper, the predicted results

of his analysis could only show limited agreement with the experimental data due, in part, to the scarcity of data on the subject.

In the mid 1980's, new papers covering the theory of tube side condensation, along with new experimental data, solidified the basic ideas about the whole process. Papers by V.G. Rifert, [37], and D.M. Maron & S. Sideman, [38], and I.Y. Chen & G. Kocamustafaogullari, [39], provide excellent theoretical methods for predicting tube side, heat transfer behavior. For the problem to be considered in this thesis, the model proposed by Maron & Sideman will be used to determine the rate of heat transfer to the tube walls.

2.5.2 DIRECT CONTACT CONDENSATION

Direct contact steam-water condensation is a relative newcomer to the experimental and theoretical world of heat transfer. The first detailed paper on experimental results was by R.M. Thomas, [40], in 1978. Dr. Thomas used the theoretical models of T.G. Theofanous, R.N. Houze, & L.K. Brumfield, [41], as the basis for correlating the results of his experiments.

After the appearance of the Thomas results, a flurry of new investigation was initiated. The bulk of which belongs to the Italian group of G.P. Celata, M. Cumo, G.E. Farello, and G. Focardi, ([42],[43],[44],[45],&[46]).

Their experimental results were for the most part, condensation of steam, (both saturated and super heated), on a smooth, sub-cooled water interface. These experimental results provide an excellent reference point for comparison of new theoretical models and experimental data. Additional experiments on direct contact condensation have been made by A. Segev, L.J. Flanigan, R.E. Kurth, & R.P. Collier, **[47]**, and I.S. Lim, R.S. Tankin, & M.C. Yuen, **[48]**, and H.J. Kim & S.G. Bankoff,**[34] & [49]**. These papers discuss the results of experiments with steam condensation on a turbulent water interface.

For the purposes of this thesis, the results and the method of model correlation presented by Kim & Bankoff are ideal. As was the case for determining the shear stress friction factors, there is no bulk fluid Reynolds number in the liquid phase. Hence, most of the correlations found in the literature are unsatisfactory in format. The turbulence centered model of Kim & Bankoff is a function of the interface structure and is independent of the relative motion of the two fluid phases.

In passing, mention must be made of papers presented by Jung-Hoon Chun, Martin A. Shimko, & Ain A. Sonin, **[50] & [51]**. This 1986 paper presents evidence of condensation instabilities at the phase interface. The experimental results show, for reasons unknown, that an instability in

the interface can increase the heat transfer by a factor of 100. The time frame for this condensation instability is approximately 10 milliseconds. There will be no attempt to model such instabilities in the condensation because the nature of the mechanism causing the instability is unclear. The extent of the effect upon the surface area for this instability is also uncertain.

2.6 COMMENTS

The literature review has shown that there is very little material in the fields of interfacial shear stress and direct contact heat transfer for stagnant liquid situations. The literature is strongly dominated by semi-theoretical modeling and experimental correlations. The review has provided a wide range of bridging models. The bridging method used in this thesis was basically chosen because of the desire for a model with a strong theoretical background. Finally, the review has provided evidence of instability in the interface condensation process which should call attention to the uncertainty in any heat transfer model to be employed.

3 METHODS

The methods chapter is devoted to a complete presentation of all the theoretical and numerical models which are used in the analysis of the present CIWH problem. Modeling the thermal-hydraulic behavior of CIWH is difficult because many different physical mechanisms are at work. The primary driving force behind the entire process is the temperature gradient between the steam and the subcooled water. A secondary driving force is the temperature gradient between the steam and the pipe wall. As we will see in chapter 4, the pipe wall-steam temperature gradient can actually be the main force driving the entire process depending upon the geometry and auxiliary feedwater flow rates. It should be clear that the condensation phenomenon is the most important process occurring in the system. Hence, it is vital that we have a good model available to predict the condensation rates as a function of position and time.

This chapter is broken into 6 sections. Section 3.1 is concerned with the overall geometry model for the system, the control volume. This is the model which will form the basis for all of our calculations. Section 3.2 will deal with the determination of the physical structure of the phase interface. Specifically, the determination of wave frequency, wave amplitude, and wave number. These three quantities are important for the determination of the interfacial heat

transfer coefficients and the onset of bridging.

Section 3.3 will be concerned with the actual estimation of the heat transfer at the phase interface and on the pipe wall. In addition, a model will be presented for determination of the minimum possible phase interface surface temperature. This model will have implications for the magnitude of the interfacial heat & mass transfer, and subsequently, the total mass flow rate of steam in the pipe.

Section 3.4 will be centered upon the calculation of the pressure gradient, and implicitly, the axial temperature gradient of the steam inside the pipe, and section 3.5 will provide a brief discussion of the interface stability model along with the model requirements. Finally, section 3.6 will take a look at the computer program used to implement the total CIWH model. This will include a discussion of the code input requirements as well as the code operational flow.

3.1 CONTROL VOLUME

The goal for the control volume approach to the CIWH problem is to provide a method of estimating the average velocity of the steam as a function of axial position in the horizontal piping system. Figure 8 gives us a perspective view of the typical control volume to be used.

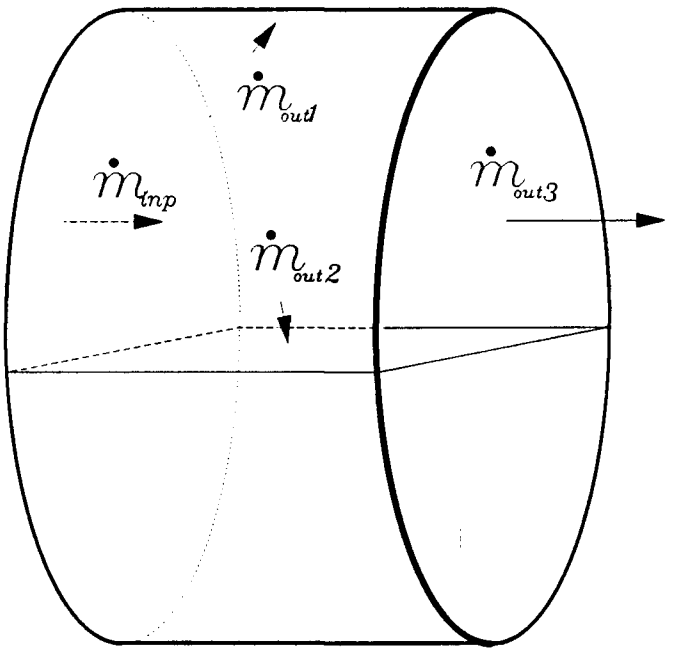

Figure (8): Control Volume

The mass flow rates are for the gas phase. Conservation of mass requires the following:

Equation (1):

$$\dot{m}_{inp} = \dot{m}_{out}$$

where:

Equation (2):

$$\dot{m}_{out} = \dot{m}_{out1} + \dot{m}_{out2} + \dot{m}_{out3}$$

These two equations merely state that there is a balance between the mass transfer modes of the control volume. The balance is between the mass which enters the control volume as steam and then exits the control volume, either directly as steam or as condensate on the pipe walls and at the phase

interface.

Figure 9 shows the control volume for the steam terminal boundary. Again, as in Figure 4, the mass flow rates are for the gas phase.

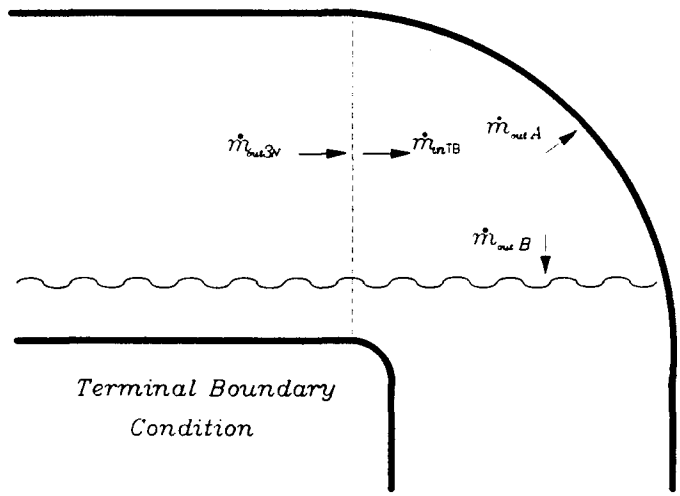

Figure (9): Terminal Boundary

Where conservation of mass is expressed by the following:

Equation (3):

$$\dot{m}_{inTB} = \dot{m}_{outA} + \dot{m}_{outB}$$

As before, this equation states that the steam mass flow rate that enters the terminal boundary must equal the condensation mass flow rates on the pipe walls and phase interface. The numerical solution approach will be to start at the steam terminal boundary and calculate the condensation mass flow rate demand on the pipe walls and phase interface. Using equation (3), we can then determine the steam mass flow rate demand into the terminal boundary control volume. The

solution method then proceeds back, axially to the steam source, calculating the steam mass flow rate as a function of axial position. Figure 10 shows the relationships needed for this process.

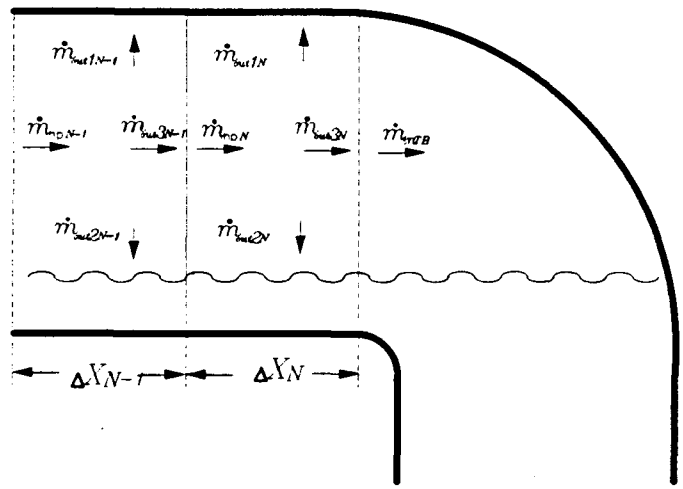

Figure (10): Mass Flow Rates

Because control volume (N), (where N is the numerical index for the total number of discrete control volumes in the horizontal pipe section), and the terminal boundary share a common border, the following conservation of mass must hold:

Equation (4):

$$\dot{m}_{out3(N)} = \dot{m}_{inTB}$$

Likewise, the following conservation of mass requirement defines the common borders for all other control volumes:

Equation (5):

$$\dot{m}_{out3(N-1)} = \dot{m}_{inp(N)}$$

Now we will begin to take a closer look at the terminal boundary. Equation (3) relates the two condensation mass transfer rates to the total mass demand into the terminal boundary control volume. The following equations describe the energy transfer which is associated with the mass transfer for the wall and interface condensation. Hence, we have:

Equation (6):

$$q_{(outA)} = h_{(outA)} A_{(outA)} \Delta T_{(outA)}$$

Equation (7):

$$q_{(outB)} = h_{(outB)} A_{(outB)} \Delta T_{(outB)}$$

Equation (8):

$$q_{(outA)} = \dot{m}_{(outA)} h_{fg(outA)}$$

Equation (9):

$$q_{(outB)} = \dot{m}_{(outB)} h_{fg(outB)}$$

where:

h_{fg} = *the latent heat of vaporization*

Now, by combining equations (6&8) and (7&9), we arrive at expressions for the mass demand of condensation, for the terminal boundary, on the pipe wall and phase interface given by the following:

Equation (10):

$$\dot{m}_{(outA)} = \frac{h_{(outA)} A_{(outA)} \Delta T_{(outA)}}{h_{fg(outA)}}$$

Equation (11):

$$\dot{m}_{(outB)} = \frac{h_{(outB)} A_{(outB)} \Delta T_{(outB)}}{h_{fg(outB)}}$$

Now, substituting into equation (3), we get:

Equation (12):

$$\dot{m}_{(inTB)} = \frac{h_{(outA)} A_{(outA)} \Delta T_{(outA)}}{h_{fg(outA)}} + \frac{h_{(outB)} A_{(outB)} \Delta T_{(outB)}}{h_{fg(outB)}}$$

However, the latent heat of vaporization is the same for the condensation on the pipe wall and at the interface. Hence:

Equation (13):

$$h_{fgTB} = h_{fg(outA)} = h_{fg(outB)}$$

Therefore, upon substitution we get:

Equation (14):

$$\dot{m}_{(inTB)} = \frac{1}{h_{fgTB}} [h_{(outA)} A_{(outA)} \Delta T_{(outA)} + h_{(outB)} A_{(outB)} \Delta T_{(outB)}]$$

Now, because of equation (4), we have the link to control volume (N). Hence, upon substitution into equation (2), once again, only the mass demand on the pipe wall and phase interface needs to be determined. In a manner similar to that used at the terminal boundary, we need to write the mass flow rate demand in terms of the energy transfer. Therefore, we get the following:

Equation (15):

$$q_{outl(N)} = h_{outl(N)} A_{outl(N)} \Delta T_{outl(N)}$$

Equation (16):

$$q_{out2(N)} = h_{out2(N)} A_{out2(N)} \Delta T_{out2(N)}$$

Equation (17):

$$q_{outl(N)} = \dot{m}_{outl(N)} h_{fg(outl(N))}$$

Equation (18):

$$q_{out2(N)} = \dot{m}_{out2(N)} h_{fg(out2(N))}$$

where:

h_{fg} = *the latent heat of vaporization*

Now, by combining equations (15&17) and (16&18), we arrive at expressions for the mass demand of condensation, for control volume (N), on the pipe wall and phase interface given by the following:

Equation (19):

$$\dot{m}_{outl(N)} = \frac{h_{outl(N)} A_{outl(N)} \Delta T_{outl(N)}}{h_{fg(outl(N))}}$$

Equation (20):

$$\dot{m}_{out2(N)} = \frac{h_{out2(N)} A_{out2(N)} \Delta T_{out2(N)}}{h_{fg(out2(N))}}$$

However, the latent heat of vaporization is the same for the condensation on the pipe wall and at the interface. Hence:

Equation (21):

$$h_{fg(N)} = h_{fg(out1(N))} = h_{fg(out2(N))}$$

Therefore, upon substitution of equation (21), we get an expression for the mass flow rate demand, into control volume (N), as follows:

Equation (22):

$$\dot{m}_{inp(N)} = \frac{1}{h_{fg(N)}}[h_{out1(N)}A_{out1(N)}\Delta T_{out1(N)} + h_{out2(N)}A_{out2(N)}\Delta T_{out2(N)}] + \dot{m}_{out3(N)}$$

Combining equations (5,14,&22), we can proceed to calculate the mass flow rate demand for steam as a function of axial pipe position. Because the interfacial stability criterion is a function of the relative motion of the fluids, we need to convert the mass flow rate demand into the average velocity field of the steam in the pipe system.

3.1.1 AVERAGE VELOCITY FIELD

In order to arrive at an expression for the average velocity field of the steam, we must begin with the definition of mass flux given by the following:

Equation (23):

$$\dot{m} = \int_S \rho(\hat{v} \cdot \hat{n})dS$$

Where S is the notation for a general curvilinear surface. For the case of steam flow through the previously defined control volume, the surface through which mass is transferred from control volume (N-1) to (N), is planer.

The orientation of the surface S is normal to the axis of the horizontal piping system. Therefore, we can represent the above surface integral as an integral over a defined area as follows:

Equation (24):

$$\dot{m} = \int_A \rho(\hat{v} \cdot \hat{n}) dA$$

Because the mass transfer along the axial direction is being treated as one-dimensional, and because the unit normal vector of area A is parallel to the direction of the velocity vector, we can make the following assumption:

Equation (25):

$$\bar{v}_{ave} = (\hat{v} \cdot \hat{n})$$

Therefore, we get:

Equation (26):

$$\dot{m} = \int_A \rho \bar{v}_{ave} dA$$

Now, because the cross-sectional area is a function of time, we need to make the following quasi-steady state assumption. Over a given time interval, there exists some average cross-sectional area for the steam to move through. The average cross-sectional area can then be assumed to be constant over the duration of the time interval. How one determines the average cross-sectional area is the subject of section 3.1.2. Therefore, applying this

assumption we get the following:

Equation (27):

$$\dot{m} = \int_{A_{ave(g)}} \rho \bar{v}_{ave} dA$$

Because the cross-sectional area is assumed to be constant over the time interval, the density and velocity can be assumed to be independent of the average cross-sectional area. Hence, we get:

Equation (28):

$$\dot{m} = \rho \bar{v}_{ave} \int_{A_{ave(g)}} dA$$

Also, because the cross sectional area is assumed to be constant over the time interval, we get for the average gas cross-sectional area the following:

Equation (29):

$$A_{ave} = \int_{A_{ave(g)}} dA$$

Therefore, upon substitution and rearranging, we get:

Equation (30):

$$\bar{v}_{ave} = \frac{\dot{m}}{\rho A_{ave(g)}}$$

This result can be shown in discretized form as:

Equation (31):

$$\bar{v}_{ave(N)} = \frac{\dot{m}_{inp(N)}}{\rho_{(N)} A_{ave(g)}}$$

Now that we have an expression for the average velocity as a function of axial position, we need to discuss how to determine the average cross-sectional area for a given time interval.

3.1.2 AVERAGE CROSS-SECTIONAL AREA

Under the premise of a horizontal piping system, it is reasonable to assume that the average cross-sectional area of flow will be independent of axial position in the system. Hence, we need only confine the determination of average cross-sectional area to the macroscopic point of view of the entire system.

At any given time t, there will be some finite quantity of liquid in the system such that the following criterion is met:

Equation (32):

$$0 \leq V_l \leq V_{tot}$$

where:

V_l = *system liquid volume*

V_{tot} = *internal volume of the pipe system*

From the prior determination of mass flow rates above, we can determine the volumetric flow rate of condensate into the liquid phase. Also, we are given the auxiliary

feedwater flow rate. Hence, adding these terms gives us the total volumetric flow rate of liquid into the piping system. This total flow rate is given by:

Equation (33):

$$\dot{V}_{tot(t)} = \dot{V}_{aux(t)} + \dot{V}_{1(t)} + \dot{V}_{2(t)}$$

where:

$\dot{V}_{tot(t)}$ = *total volumetric flow rate of liquid at time t*

$\dot{V}_{aux(t)}$ = *aux feedwater volumetric flow rate at time t*

$\dot{V}_{1(t)}$ = *vol. flow rate of condensation from pipe wall at time t*

$\dot{V}_{2(t)}$ = *vol. flow rate of condensation at phase interface at time t*

We will now assume that, for short time intervals, the volumetric flow rate remains constant. Hence, we can extrapolate, by integration over the time interval, to determine the total increase in liquid phase volume in the piping system for the time interval. This is given by:

Equation (34):

$$V_{\Delta t} = \int \dot{V}_{tot(t)} dt$$

where:

$V_{\Delta t}$ = *liquid volume increase during the time interval t*

Therefore, the total volume of liquid at the end of time interval t is given by the following:

Equation (35):

$$V_{tot(t+1)} = V_{tot(t)} + V_{\Delta t}$$

Now that we have the liquid volume at the start and end of time interval t, we will assume that the average volume for this time interval is given by the following:

Equation (36):

$$V_{ave} = \frac{V_{tot(t)} + V_{tot(t+1)}}{2}$$

Now that we have determined the average volume of liquid in the pipe system, we will take advantage of the above stated cross-sectional area independence in axial position. If we take the average liquid volume in the pipe and divide by the total length of the pipe, we get:

Equation (37):

$$A_{ave(l)} = \frac{V_{ave}}{L}$$

where:

L = *total length of the pipe system*

$A_{ave(l)}$ = *average cross-sectional area of liquid*

Hence, we can now determine the average cross-sectional area of the steam phase by the following expression:

Equation (38):

$$A_{ave(g)} = A_{tot} - A_{ave(l)}$$

where:

A_{tot} = *total cross-sectional area of the pipe*

3.1.3 HEAT TRANSFER SURFACE AREAS

With the average cross-sectional area of the gas phase determined, we will now move on to determine the surface areas on the pipe wall and at the phase interface

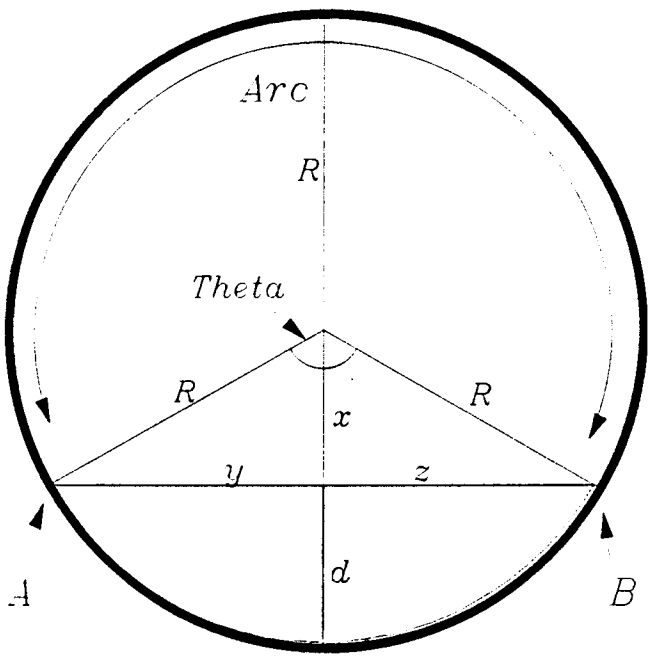

Figure (11): Cross-Section: d<R

Figure 11 shows us the cross-sectional area of the piping system with both the steam and water present. From this picture, which shows that the depth of the liquid is less than the radius of the pipe, it can be seen that the heat transfer surface areas for the pipe wall is given by:

Equation (39):

$$A_{out1} = ArcL$$

where:

Arc = *distance from A clockwise to B*

L = *length of the piping system*

Likewise, the phase interface surface area is given by:

Equation (40):

$$A_{out2} = ChordL$$

where:

Chord = *linear distance from A to B*

L = *length of the piping system*

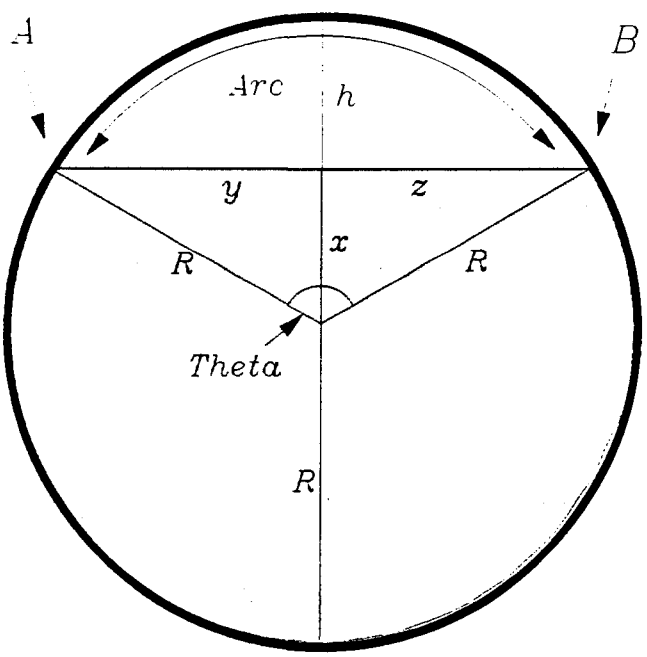

Figure (12): Cross-Section: d>R

Figure 12 shows us the cross-sectional area of the piping system for the case where the depth of the liquid phase is greater than the radius of the pipe. The above equations for heat transfer surface areas hold for both cases. However, it is necessary to have different methods of determining the arc length and chord length depending upon the depth of the liquid phase in the pipe system. We will begin with determining the chord length as follows:

Equation (41):

$$\text{Chord} = 2R\sin\left(\frac{\theta}{2}\right)$$

This expression is valid for any depth of liquid phase, yet, the method to determine theta is dependent on the liquid phase depth. The expression for theta is given by:

Equation (42):

$$\Theta = 2\cos^{-1}\left\{\frac{(R-d)}{R}\right\}$$

for: $d \leq R$

or

Equation (43):

$$\Theta = 2\cos^{-1}\left\{\frac{(d-R)}{R}\right\}$$

for: $d \geq R$

where:

$R = pipe\ radius$

$d = liquid\ depth$

Now that we have the necessary expressions for theta, it is a simple matter to define the length of the arc from point A to point B as:

Equation (44):

$$Arc = 2\pi R - R\Theta$$

for: $d \leq R$

or

Equation (45):

$$Arc = R\Theta$$

for: $d \geq R$

We now have expressions for the heat transfer surface area for the pipe wall and phase interface. However, the form is for the entire system. That is easily dealt with by replacing the total length of the pipe system with the length of control volume (N). That will give the following definitions for each discrete control volume as:

Equation (46):

$$A_{out1} = Arc\Delta X_N$$

Equation (47):

$$A_{out2} = Chord\Delta X_N$$

A brief note is in order about the heat transfer surface areas in the terminal boundary control volume. It is assumed that the pipe wall surface area and the phase interface surface area are determined in the same way as all other discrete control volumes. The only difference is in the definition of delta X. For the terminal boundary, the following expressions apply:

Equation (48):

$$A_{outA} = ArcD$$

Equation (49):

$$A_{out2} = ChordD$$

where:

D = *pipe diameter*

That completes the determination of expressions for all heat transfer and cross-sectional areas. The evaluation of heat transfer coefficients and temperature gradients will be discussed in section 3.3.

3.2 INTERFACE STRUCTURE

The determination of the phase interface structure is important for two reasons. The primary reason is to determine the wave number as a function of axial position in the piping system. The wave number is an important input value for the bridging criterion because it defines the onset of bridging for a given value of relative phase motion. The second reason for determining the interface structure involves estimation

of the wave amplitude as a function of axial piping position. The wave amplitude is an integral component of the turbulence centered model for the interfacial heat transfer coefficient, which will be discussed in greater detail in section 3.3.

Because there is no theoretical model for determining the wave amplitude and wave number on the phase interface, it will be necessary to use experimental data to develop correlations for these quantities. For this thesis, the wave amplitude correlation will be a function of wave frequency, and the wave number model will require knowledge of the rate of change in wave frequency as a function of axial piping position.

3.2.1 INTERFACE WAVE FREQUENCY AND AMPLITUDE

Because there are no theoretical models to estimate the wave frequency, we are forced to develop a correlation for the frequency. Preferably, the correlation will be a function of a dimensionless group so that we might apply the correlation, with some confidence, to regions which are outside of the original correlation data.

It turns out that the only source available for raw interface structure data is the work by Kim, [34]. This report provides raw data for wave frequency and wave amplitude with respect to additional data on geometry, fluid physical properties, and flow conditions. This report also has the only data on this subject which is relevant

to the present analysis. The data is for a horizontal, counter-current flow situation of steam and subcooled water which is directly applicable to the present work. One major draw back of the experiment, with respect to the current analysis, is that the liquid phase was flowing along the axis of the test section. That is quite different from the present case which has no axial fluid motion. Therefore, one must use some discretion in applying the methods of this thesis to any particular case analysis.

With the need for a dimensionless group to formulate a correlation, we initially looked to the familiar Euler number, (Eu), and Weber number, (We). Their respective definitions are as follows:

Equation (50):

$$Eu = \frac{g \Delta P \rho_g A_g^2}{\dot{m}_g^2}$$

and

Equation (51):

$$We = \frac{\dot{m}_g^2 D_e}{g \rho_g A_g^2 \sigma}$$

where:

g = *gravitational acceleration*

A_g = *cross-sectional area of gas flow*

ρ_g = *density of gas*

$\dot{m}_g$ = *mass flow rate of gas*

ΔP = *specific pressure drop for gas*

D_e = *equivalent diameter*

σ = *surface tension*

A regression analysis was performed on all of the dimensionless groups which are presented in this section. The results of the regression analysis will be presented in terms of the correlation coefficient. A correlation coefficient value of 100 % would mean a perfect fit of the data to the regression function, and a value of 0% would mean no relationship of any kind is present. The coefficient is defined by the following:

$$C = \frac{n\sum x_i y_i - \sum x_i \sum y_i}{\left[\left(n\sum x_i^2 - \left(\sum x_i\right)^2\right)\left(n\sum y_i^2 - \left(\sum y_i\right)^2\right)\right]^{\frac{1}{2}}}$$

where:

x = *x-axis values*

y = *y-axis values*

n = *total number of data points*

The correlation coefficient for the above mentioned dimensionless groups is very poor; less than 10%. Therefore, it is necessary to develop our own dimensionless groups using the Buckingham Pi method, **[52]**. After several trials, the following groups have been selected:

Equation (52):

$$\Pi_1 = \frac{D_e \Delta\rho^{(0.4)} g^{(0.2)}}{\dot{m}_g^{(0.4)}}$$

Equation (53):

$$\Pi_2 = \frac{T_g}{T_f}$$

Equation (54):

$$\Pi_3 = \frac{\bar{v}_{ave}}{af}$$

where:

g = *gravitational acceleration*

$\dot{m}_g$ = *mass flow rate of gas*

D_e = *equivalent diameter*

$\Delta\rho$ = *density difference of gas-liquid*

T_g = *temperature of gas*

T_f = *temperature of liquid*

$\bar{v}_{ave}$ = *average velocity of gas*

a = *wave amplitude*

f = *wave frequency*

Figure 13 and Figure 14 show the results of the data correlations. The parameter on the x-axis for both figures is given by the following:

Equation (55):

$$\Pi = \Pi_1^{(0.1)} \exp\left(\frac{\Pi_2}{125000}\right)$$

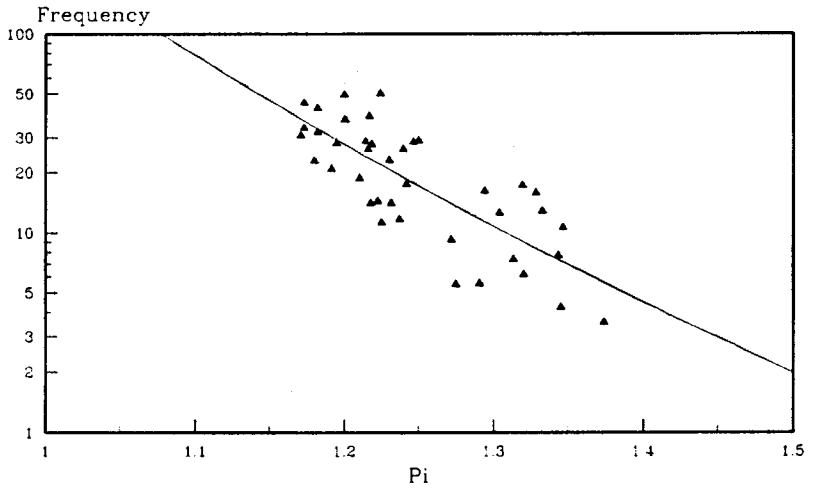

Figure (13): Frequency Correlation

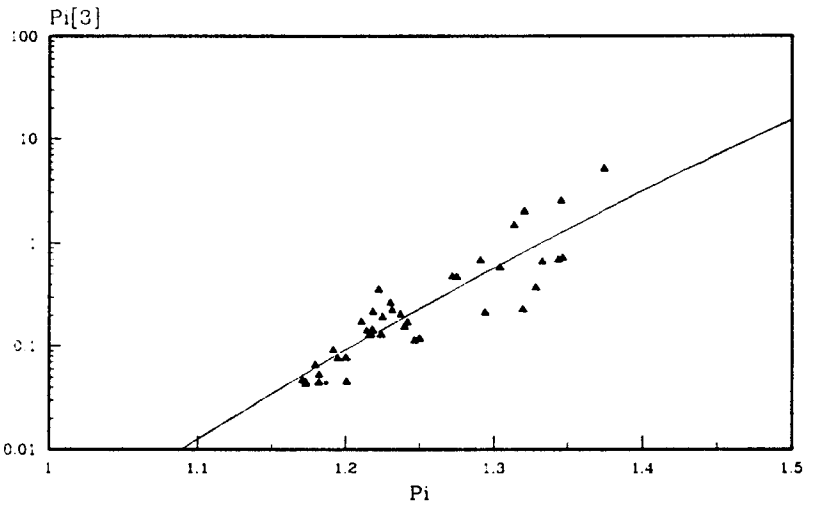

Figure (14): Amplitude Correlation

The correlation for frequency is given by:

Equation (56):

$$f = 241.14631\,\Pi^{-11.82684}$$

The correlation factor for this expression is 77.9%.

The correlation for Π_3 is given by:

Equation (57):

$$\Pi_3 = 0.0014128\Pi^{22.89843}$$

The correlation factor for this expression is 89.6%. Once this expression is evaluated, the amplitude can be found by the following:

Equation (58):

$$a = \frac{\bar{v}_{ave}}{f\Pi_3}$$

3.2.2 INTERFACE WAVE NUMBER

Because there are no theoretical models to estimate the wave number as a function of position, we will need to develop a correlation for one, or develop a theoretical model. There are, unfortunately, no experimental data to develop such a correlation. Therefore, we are left to develop a theoretical model.

The task of creating a new theoretical model is very extensive and could be the sole topic of a thesis on its own. Therefore, we need to make the following assumption: All waves which impact the terminal boundary pipe wall are completely damped. This will eliminate the need to consider wave reflection along with constructive and destructive interference of waves traveling counter-current to the steam flow.

We will start by defining the wave number as:

Equation (59):

$$k = \frac{f}{c}$$

where:

$c =$ *wave velocity*

We are interested in deriving a relationship which will allow us to determine the rate of change in wave number as a function of position. We will also make the assumption that the wave velocity is equal to the inlet steam velocity. We will make this assumption purely for the sake of simplicity because there is no available data on this particular topic. Taking the derivative of the wave number with respect to position we get:

Equation (60):

$$\frac{d}{dx}(k) = \frac{1}{\bar{v}_{ave_{(0)}}} \frac{d}{dx}(f)$$

In approximate form we get:

Equation (61):

$$\Delta k \approx \frac{1}{\bar{v}_{ave_{(0)}}} \Delta f$$

And in discrete nodal form we have:

Equation (62):

$$k_{(N)} = k_{(N-1)} + \frac{1}{\bar{v}_{ave_{(0)}}} (f_{(N)} - f_{(N-1)})$$

with Boundary Conditions:

$$k(L) = 0$$

$$f(L) = 0$$

These expressions will allow us to estimate the wave number as a function of position at each time interval.

3.3 HEAT TRANSFER

This section will be concerned with the two major modes of heat transfer from the steam to the subcooled liquid. Also, the mixing of condensate with the liquid which is present in the system will be addressed.

3.3.1 PIPE WALL HEAT TRANSFER

In this section, we will be discussing the method used to determine heat transfer coefficients, $h_{(outIN)}$ & $h_{(outIA)}$, from the steam to the pipe wall. The method used by Maron and Sideman, [38], will be used in this thesis. Figure 15 shows the cross-sectional view of the pipe.

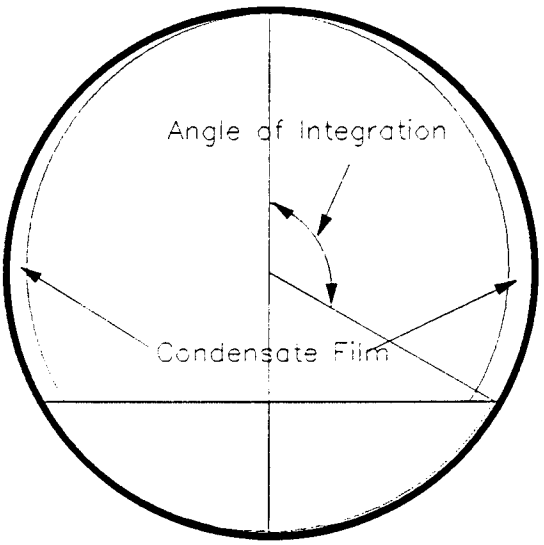

Figure (15): Pipe Wall Condensation

According to Maron and Sideman, the local heat transfer coefficient is given by the following:

Equation (63):

$$h_\phi = C_1 \left(\frac{\sin \phi}{\phi} \right)^{0.25}$$

and:

Equation (64):

$$C_1 = \left(\frac{g h_{fg} \rho_l^2 k_l^3}{4 \mu_l R \Delta T} \right)^{0.25}$$

where:

g = *gravitational acceleration*

ρ_l = *liquid density*

k_l = *liquid thermal conductivity*

μ_l = *liquid viscosity*

R = *pipe radius*

h_{fg} = *latent heat of vaporization*

ΔT = *wall surface subcooling*

Now, all that needs to be done is to integrate over the pipe wall surface length and then divide by the angle of integration to get the average heat transfer coefficient on the pipe wall. Hence:

Equation (65):

$$\mathbf{h}_{(outA)} = \mathbf{h}_{(outN)} = \frac{2C_1}{(\pi-\phi_m)} \int_0^{(\pi-\phi_m)} \left(\frac{\sin\phi}{\phi}\right)^{0.25} d\phi$$

This integral is then evaluated numerically at each time interval by the use of the extended trapezoid rule. The integral then becomes:

Equation (66):

$$\int_0^{(\pi-\phi_m)} \left(\frac{\sin\phi}{\phi}\right)^{0.25} d\phi = \frac{(\pi-\phi_m)}{N-1} \left\{ \frac{1}{2}(f_1 + f_N) + \sum_{i=2}^{N-1} f_i \right\}$$

where:

$N-1$ = *number of cells*

3.3.2 PHASE INTERFACE HEAT TRANSFER

In this section we will concentrate upon the method of calculating the heat transfer coefficients at the phase interface, $\mathbf{h}_{(out2N)}$, & $\mathbf{h}_{(outB)}$. This thesis will be using the turbulence centered model of Kim, [34], to determine the value of the Nusselt number. The following expression gives the correlation for the Nusselt number as:

Equation (67):

$$Nu_t = 0.134 Re_t^{0.95} Pr^{0.5}$$

The turbulent Reynolds number is defined as:

Equation (68):

$$Re_t = \frac{u_t a}{\nu}$$

where:

a = *wave amplitude*

ν = *kinematic liquid viscosity*

$$u_t = \sqrt{\frac{\tau_i}{\rho}}$$

The shear stress is given as:

Equation (69):

$$\tau_i = \tau_{i,a} - \frac{\bar{v}_{ave}}{\text{Chord}} \frac{d\dot{m}_g}{dx}$$

where:

$\dot{m}_g$ = *steam mass flow rate*

An expression for the adiabatic interfacial shear stress can be found in section 3.4. Once we have determined the turbulent Nusselt number, we can determine the interface heat transfer coefficient as:

Equation (70):

$$h_{(out2N)} = h_{(outA)} = \frac{k}{a} Nu_t$$

where:

k = *liquid thermal conductivity*

a = *wave amplitude*

3.3.3 LIQUID MIXING

Because of the mass transfer at the phase interface and on the pipe wall, it is necessary to estimate how this saturated liquid from the condensation process will interact with the subcooled liquid. The main point of this is to estimate the surface temperature of the liquid phase as a function of time. For the purpose of this thesis, we will assume that the condensate will be uniformly and completely mixed with the subcooled liquid phase. This assumption will allow us to estimate the minimum possible liquid phase surface temperature because the condensate cannot mix with more liquid than is present at any given time. Another more complex approach to the mixing probem would be to assume only a small layer of condensate mixing with convection to the rest of the liquid. This method, however, will not be used here.

In addition to the uniform mixing assumption, we will assume that the latent heat of vaporization which is associated with the condensation on the pipe wall will be completely absorbed and then conducted away by the pipe

wall. Also, for the sake of simplicity, we will assume that the enthalpy values for all of the individual mass groups is independent of time.

We will begin by formulating the energy balance relationship as follows:

Equation (71):

$$\frac{d}{dt}(m_{tot}h_{tot}) = \frac{d}{dt}(m_{AF}h_{AF}) + \frac{d}{dt}(m_{c1}h_{c1}) + \frac{d}{dt}(m_{c2}h_{c2}) + \frac{d}{dt}(m_{c2}h_{fg})$$

where the subscripts are associated to the following mass groups:

tot = *total mass for the system*

AF = *auxiliary feedwater*

$c1$ = *condensate from the pipe wall*

$c2$ = *condensate on the interface*

Now, carry out the differentiation. Also, if we assume that the latent heat of vaporization and the enthalpy of the auxiliary feedwater are independent of time, we get the following:

Equation (72):

$$m_{tot}\frac{dh_{tot}}{dt} + h_{tot}\frac{dm_{tot}}{dt} = h_{AF}\frac{dm_{AF}}{dt} + h_{c1}\frac{dm_{c1}}{dt} + \frac{dm_{c2}}{dt}(h_{c2} + h_{fg})$$

If we substitute the following thermodynamic relationship:

Equation (73):

$$dh_{tot} = C_{ptot} dT_{tot}$$

and

Equation (74):

$$\frac{dm}{dt} = \dot{m}$$

we will get the following:

Equation (75):

$$\frac{dT_{tot}}{dt} = \frac{1}{m_{tot} C_{ptot}} (-h_{tot} \dot{m}_{tot} + h_{AF} \dot{m}_{AF} + h_{cl} \dot{m}_{cl} + \dot{m}_{c2}(h_{c2} + h_{fg}))$$

Now we can solve this for the total change in liquid phase temperature over time interval Δt as the following:

Equation (76):

$$\Delta T_{tot} = \frac{\Delta t}{m_{tot} C_{ptot}} (-h_{tot} \dot{m}_{tot} + h_{AF} \dot{m}_{AF} + h_{cl} \dot{m}_{cl} + \dot{m}_{c2}(h_{c2} + h_{fg}))$$

3.4 RESSURE GRADIENT

Calculation of the pressure gradient for the steam phase is necessary to allow the determination of the physical properties. The pressure drop model that will be used in this thesis is the one presented by Kim [34]. Figure 16 shows the two different shear stress components which need to be accounted for.

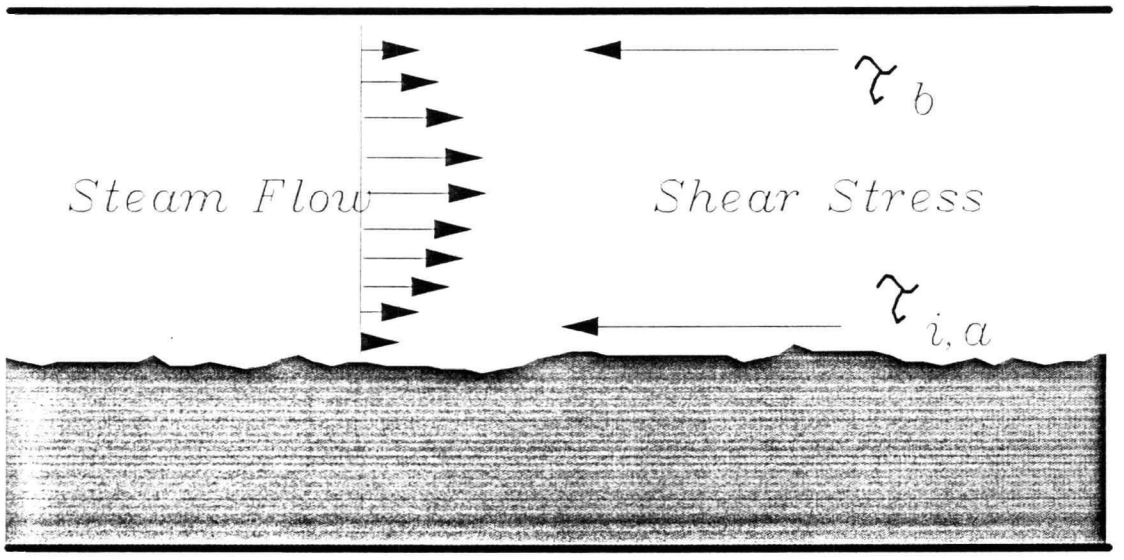

Figure (16): Interface & Wall Shear Stress

From [34], the following expression for the pressure gradient has been taken:

Equation (77):

$$\frac{dP_g}{dx} = \frac{dP_g}{dx}_a - \rho_g \bar{V}_{ave} \frac{d\bar{v}_{ave}}{dx}$$

where:

$\frac{dP_g}{dx}_a$ = *frictional losses of the system*

$\rho_g \bar{V}_{ave} \frac{d\bar{v}_{ave}}{dx}$ = *frictional losses due to mass transfer*

From [34], the following definitions are used:

Equation (78):

$$\frac{dP_g}{dx}_a = \frac{-1}{D-d}(\tau_{i,a} + \tau_b) - \rho_g g \sin\theta$$

However, the system we are looking at is horizontal. Therefore, the second term on the right hand side goes to zero and the equation becomes:

Equation (79):

$$\frac{dP_g}{dx}\Big|_a = \frac{-1}{D-d}(\tau_{i,a} + \tau_b)$$

The calculation of the shear stress is given by:

Equation (80):

$$\tau_b = f_b \rho_g \frac{\bar{v}_{ave}^2}{2}$$

where:

τ_b = *wall shear stress*

The wall friction factor is given by:

Equation (81):

$$f_b = 0.079 Re_{g,D_e}^{-0.25}$$

The Reynolds number is defined as:

Equation (82):

$$Re_{g,D_e} = \frac{\rho_g \bar{v}_{ave} D_e}{\mu_g}$$

where:

D_e = *equivalent diameter*

or

Equation (83):

$$D_e = 4\left\{\frac{\text{cross-sectional area of flow}}{\text{wetted perimeter}}\right\}$$

The interfacial shear stress is given by:

Equation (84):

$$\tau_{i,a} = f_{i,a} \rho_g \frac{\bar{v}_{ave}^2}{2}$$

The interfacial friction factor is given by:

Equation (85):

$$f_{i,a} = 1.875 * 10^{-5} Re_f + 0.0068$$

for:

$$Re_f < 340$$

However, because the liquid phase Reynolds number is zero, the interfacial friction factor is given by:

Equation (86):

$$f_{i,a} \approx 0.0068$$

Therefore, upon substitution, we get the following:

Equation (87):

$$\frac{dP_g}{dx} = \frac{-1}{D-d}[\tau_{i,a} + \tau_b] - \rho_g \bar{V}_{ave} \frac{d\bar{v}_{ave}}{dx}$$

Equation (88):

$$\frac{dP_g}{dx} = \frac{-1}{D-d}\left[f_{i,a}\rho_g \frac{\bar{v}_{ave}^2}{2} + f_b \rho_g \frac{\bar{v}_{ave}^2}{2} \right] - \rho_g \bar{V}_{ave} \frac{d\bar{v}_{ave}}{dx}$$

Equation (89):

$$\frac{dP_g}{dx} = \frac{-\rho_g \bar{v}_{ave}^2}{2(D-d)}[f_{i,a} + f_b] - \rho_g \bar{V}_{ave} \frac{d\bar{v}_{ave}}{dx}$$

Now, we need to place the pressure gradient into a discrete, nodal format. Therefore:

Equation (90):

$$\frac{\Delta P_{g(N)}}{\Delta x_{(N)}} = \frac{-\rho_{g(N)} \bar{v}_{ave(N)}^2}{2(D-d)}[f_{i,a(N)} + f_{b(N)}] - \rho_{g(N)} \bar{V}_{ave(N)} \frac{\Delta \bar{v}_{ave(N)}}{\Delta x_{(N)}}$$

Hence, the change in pressure over a given node (N) is given by:

Equation (91):

$$\Delta P_{g(N)} = \frac{\Delta P_{g(N)}}{\Delta x_{(N)}} \Delta x_{(N)}$$

We can now determine the pressure field in the steam, by starting at the steam inlet and proceeding to the terminal boundary, using the following expression:

Equation (92):

$$P_{\left(N-\frac{1}{2}\right)} = P_{\left(N-\frac{1}{2}\right)} - |\Delta P_{(N)}|$$

where:

$$P_{\left(N-\frac{1}{2}\right)} = P_{inlet} \quad for \ the \ first \ node$$

Once the pressure field is established, the physical properties of the steam as a function of position can be determined. Note: (This is done using an iterative process within a time interval to converge the heat transfer coefficients and pressure field. More about this is contained in section 3.6.)

3.5 BRIDGING

For this thesis, we will be using the transition model of Ahmed & Banerjee, **[21]**. Their paper provides a nonlinear stability criterion for the onset of bridging. This section will outline the solution method used and present the final result for the onset of bridging. Figure 17 Shows the physical layout reference for the derivation.

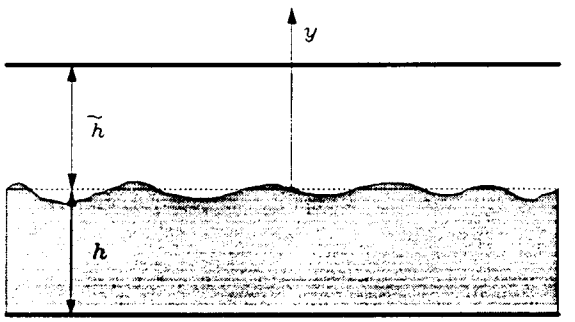

Figure (17): Bridging Model Geometry

The derivation begins with the Laplace equation for wave propagation which is given by the following:

Equation (93):

$$\nabla^2 \Phi = 0$$

and

Equation (94):

$$\nabla^2 \tilde{\Phi} = 0$$

where:

Φ = *total velocity potential of liquid*

$\tilde{\Phi}$ = *total velocity potential of gas*

These equations are subject to the following boundary conditions:

Equation (95):

$$\frac{\partial \Phi}{\partial y} = 0$$

for: $y = -h$

and

Equation (96):

$$\frac{\partial \tilde{\Phi}}{\partial y} = 0$$

for: $y = +\tilde{h}$

where:

$\tilde{h}$ = *distance from gas-liquid interface to pipe-gas interface*

h = *distance from gas-liquid interface to pipe-liquid interface*

Using a perturbation technique based on the method of multiple scales, it is possible to convert the general solution to the Laplace equation into multiple equations containing like powers of ϵ, which is the perturbation variable. The multiple equations of epsilon allow for different order approximations to the solution. Solving the first order epsilon equation will lead to a first order, or linear approximation to the solution of the governing equations. Hence, solving higher order epsilon equations leads to higher order, non-linear approximations to the exact solution. The first order linear solution to the Laplace equations results in the following linear stability criterion:

Equation (97):

$$G(\tilde{\sigma} + \rho'\sigma) - k\rho'(v - \tilde{v})^2 \geq 0$$

where:

k = *wave number*

v = *liquid velocity*

$\tilde{v}$ = *gas velocity*

$$\rho' = \frac{\tilde{\rho}}{\rho}$$

ρ = *liquid density*

$\tilde{\rho}$ = *gas density*

$$G = g(1 - \rho')$$

$$\sigma = \tanh(kh)$$

$$\tilde{\sigma} = \tanh(k\tilde{h})$$

If the above condition is not satisfied, this gives rise to linear Kelvin-Helmholtz instability.

Ahmed and Banerjee have shown that the third order perturbation expansion leads to a non-linear Schrodinger equation. The stability of the system is found to be dependent upon the sign of the coefficients to the solution to this particular Schrodinger equation. Of primary importance is the sign of the coefficient beta, given as follows:

Equation (98): $\beta \geq 0$

with

Equation (99):

$$\beta = \frac{-(\nu\tilde{\sigma}\omega_1 + \rho'\sigma\tilde{v}\omega_2)}{2Gk(\rho'\sigma\omega_2 + \tilde{\sigma}\omega_1)}$$

where:

ω_1 = *function defined by the cited reference*

ω_2 = *function defined by the cited reference*

ν = *function defined by the cited reference*

If the above criterion is not satisfied, this gives rise to a non-linear Kelvin-Helmholtz instability.

As mentioned in section 2.3.1, this particular bridging criterion is capable of predicting the onset of slug flow at relative velocities well below those of linear Kelvin-Helmholtz models. This model is also in better agreement with the broad range of experimental results than any of the other bridging models discussed in chapter 2.

3.6 CODE OPERATIONS

In this section, we will focus on the numerical flow process, and upon the steps necessary to execute the program. The code has been written using the software package Lotus Symphony, **[53]**. Because of the extreme size of the code, (over 20,000 cell addresses), it is not practical to present a hard copy of the code. Therefore, a copy of the main spreadsheet template is included on floppy disc in the appendix. Also, the size problem will limit the discussion of the code numeric operation to the approximate level of flow charting.

3.6.1 NUMERICAL FLOW

The actual execution of the code is somewhat like a FORTRAN code in the sense that the code is broken down into smaller modules called subroutines. In a spreadsheet, the subroutines are referred to as macros. On a spreadsheet, however, macros are used to control the movement of the cell operation cursor, and not the actual order of function execution. This is unlike the purpose of a subroutine in FORTRAN which is used to directly manipulate the order of function execution.

Figure 18 is a flow chart for the numerical process used in this thesis. This flow chart shows that there are two main loops within the overall time loop.

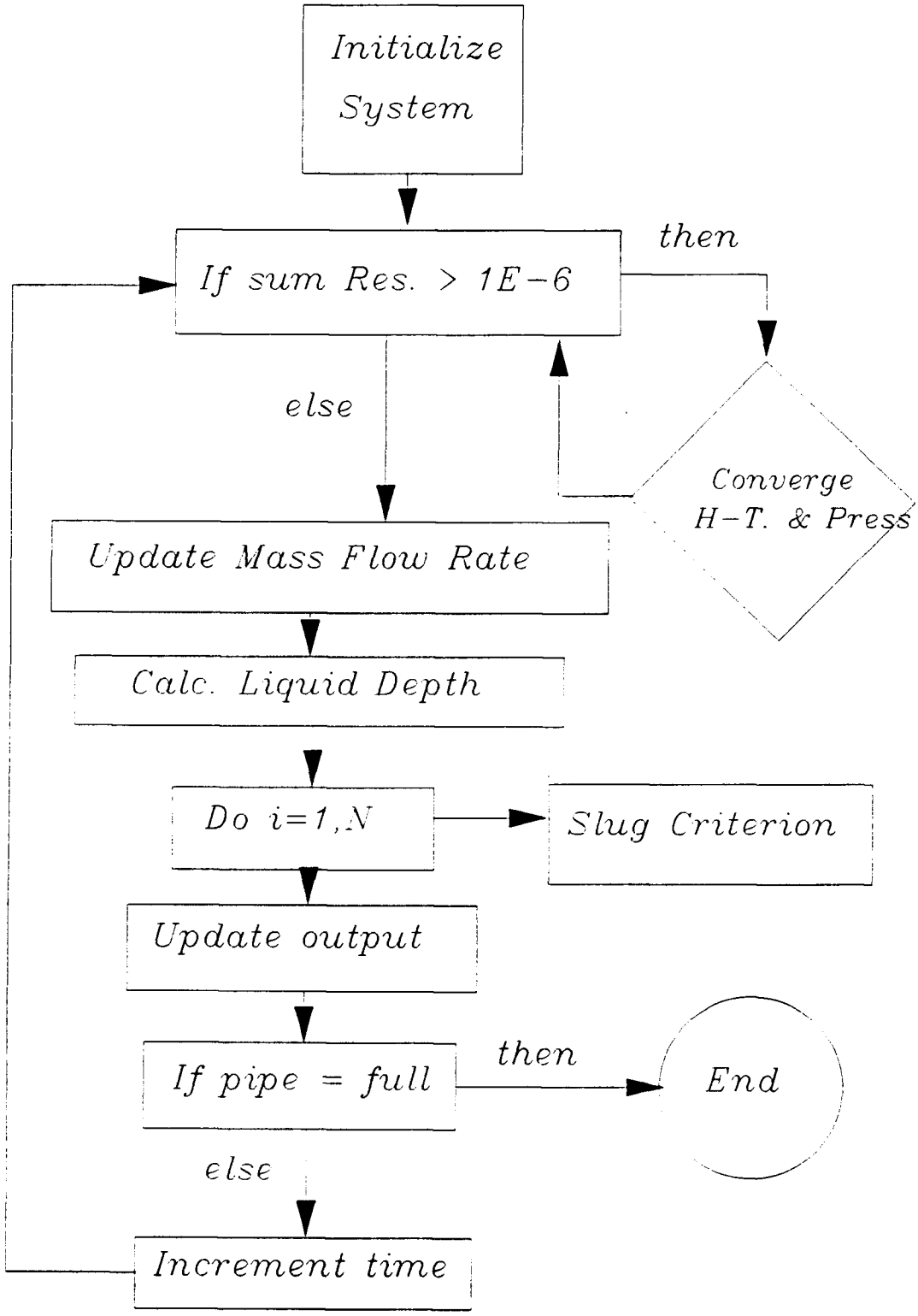

Figure (18): Numerical Flow Chart

The first loop is for the purpose of converging the heat transfer coefficients, interface temperature, and steam pressure as a function of axial pipe position. The second loop is for evaluation of the slug formation criterion at each axial node.

3.6.1.1 CONVERGENCE LOOP

As the code enters the loop for the first pass, the physical properties, heat transfer coefficient, interface temperature, and pressure drop are all being estimated by the input values which are installed during the code initialization. These initialized values reside in cell locations which can be thought of as the old value estimates. At the end of the first pass, the numerical value estimates for heat transfer coefficient, interface temperature, and pressure are copied to the location of the old value estimates. This new set of old value estimates becomes the basis of calculation for new estimates of the heat transfer coefficient, interface temperature and pressure drop. The process of copying the new estimates to the old value estimate location will continue until the numerical value of the difference between the new estimate and old estimate is below a threshold value.

The convergence loop process is applied to every node so that we have convergence as a function of position.

In order to determine the stopping point for the convergence loop, it will be necessary to define a residual by the following:

Equation (100):

$$R_n = |New_n - Old_n|$$

where:

New_n = *the new estimate at node n*

Old_n = *the old estimate at node n*

Now we will apply this definition to both the heat transfer coefficients and to the pressure field. Therefore, we have:

Equation (101):

$$R1_n = |New1_n - Old1_n|$$

and

Equation (102):

$$R2_n = |New2_n - Old2_n|$$

where:

$New1_n$ = *the new estimate of H-T coefficient*

$Old1_n$ = *the old estimate of H-T coefficient*

$New2_n$ = *the new estimate of pressure*

$Old2_n$ = *the old estimate of pressure*

$R1_n$ = *H-T coefficient residual* $R2_n$ = *pressure residual*

Using this definition of the residual, the convergence criterion is defined by the following:

Equation (103):

$$\sum_{i=1}^{N} R1_i \leq Limit$$

and

Equation (104):

$$\sum_{i=1}^{N} R2_i \leq Limit$$

where:

Limit = *numerical convergence criterion*

The above convergence criterion is then applied to the heat transfer coefficient and to the pressure field. For this work, the numerical value used for Limit is 1.0E-6.

3.6.1.2 SLUG FORMATION LOOP

The slug formation loop is very straight forward. After the heat transfer coefficients and pressure field are converged, The flow chart shows that there are intermediate steps to update the mass flow rate values. Once that has been done the slug formation loop is executed. This loop simply applies the slug formation criterion of section 3.5 to each node on the pipe axis to determine the stability status of the node.

It should be briefly noted that the slug formation loop uses a brute force method of copying the node

parameters required for stability analysis to a small section of the spreadsheet. The analysis is performed and the result is copied back to a holding cell for later output. This massive copying of data must be done for each node. The resultant effect on the execution time of the code as a whole is significant. Approximately 75% of the code operation time is spent on the movement of data for slug formation analysis. The underlying reason for all of the data copying is in the size of the slug formation criterion calculations, (approximately 2,000 cells). To have the slug formation calculation functions coupled to each cell would require in excess of 200,000 cells which is far beyond the memory capacity of the software.

3.6.2 CODE EXECUTION

The execution of the code is quite simple. The first thing one needs to do after starting Symphony is to retrieve the template worksheet. The name of the template is **"TEMPLATE.WR1"**. Once the template is in place, it is time to fill in the input requirements in the input window. Use the Symphony services menu, (F9) to select the Input window. The parameters are described by the following:

Diameter = physical diameter of the pipe in meters.

Pressure = inlet absolute steam pressure in Pascals.

AF Temp = auxiliary feedwater inlet temperature in

Kelvin.

AF Vdot = auxiliary feedwater flow rate in gallons per minute.

Wall Sub = temperature drop between steam and pipe wall in Kelvin.

Set Point= liquid height level in pipe at which you would like to change the operating parameters, (in meters). This is a termination flag for the code.

dt = size of each time step in seconds.

Length = length of the pipe system in meters.

Once you have filled in the input window parameters to your satisfaction, it is necessary to initialize the system before computation can begin. To do this, you must again use the services menu to use the Runner window. Now press the "USER" key, (F7), and enter the name of the system initialization macro, "SI", and press return. The "SI" macro will initialize the system to 100% void fraction using the parameters that have been entered in the Input window.

After the spreadsheet has been initialized, it is necessary to choose a driver to execute the program. There are two drivers to choose from. The first driver macro is named "DRIVE", and it will execute the program for a single time step only, irregardless of any Set Point value

that is in the Input window. The second driver macro is named "TD", and this macro will execute the program until the Set Point liquid height is reached for the start of a time step. Both driver macros are used through the "USER" key, (F7), like the macro "SI" was used to initialize the system.

The output for the program is written to a file on the hard drive of the computer at the following Disk Operating System, (DOS), address: C:\SYMPHONY\OUTPUT.PRN. The column output is labeled for identification.

4 RESULTS

In this chapter, we will be looking at two specific cases where CIWH is suspected of having been the cause of major piping system damage. Case 1 deals with a November 20, 1985 event at the San Onofre Nuclear Generating Station, Unit 1. The data for modeling this event are taken from **NUREG-1190**, **[54]**. Case 2 deals with the feedwater nozzle damage at Trojan Nuclear Generating Station. The data for modeling this event are taken from a report contracted by Portland General Electric, Company, (PGE), for determination of CIWH prevention, **[55]**

4.1 CASE 1: MAIN FEEDWATER LINE FILLUP

Because of a leak in the salt water condensers, the steam generators were in a blowdown mode to prevent the contamination of the steam generator tubes. Because of the blowdown operation, the main feedwater line to the steam generator was only receiving partial feedwater. After a loss of offsite power, a reactor trip was initiated and main feedwater was terminated. However, because of check valve seating failure, the feedwater line drained and became steam filled before the auxiliary feedwater pumps came on line.

4.1.1 SYSTEM DESCRIPTION

Using the chronological sequence of events table in reference **[54]**, it was possible to reconstruct the operating parameters that should be used in the numerical estimate

of the transient fillup behavior. The physical data of the layout for the main feedwater line is also from **[54]**. The main feedwater line has an inside diameter of 0.253 Meters and a linear equivalent length of 62.0 Meters. The steam pressure was at 5.24 MPa. The auxiliary feed water temperature was 300 Kelvin. The thermal subcooling between the inside pipe wall surface and the steam saturation temperature is assumed to be 0.5 Kelvin. The auxiliary feedwater flow rate was 135 gpm for 5.5 minutes and then 25 gpm for 6 minutes. After the 6 minutes of 25 gpm auxiliary feedwater, a loud bang was heard throughout most areas inside of the control room, auxiliary buildings, turbine halls, and even outside areas surrounding the reactor containment building.

4.1.2 ANALYSIS RESULTS FROM THE NRC

The result of the post-accident analysis by the NRC is as follows. The mainfeed water line was calculated to be at 1-2 percent void fraction at the time of the water hammer event. The water bridging was assumed to have occurred at the point where the feedwater line bends upward to go to the steam generator feedring nozzle, 60 Meters from the auxiliary feed water inlet to the main feedwater line.

There are no calculations of the over-pressure or forces which the main feedwater line would be subjected to due

to the slug formation at the above assumed position. All damage to the piping system is assumed to be the result of the assumed slug formation mentioned above. The forces generated by the assumed CIWH are derived from the forces needed to create the piping system support damage. The inferred over-pressure is 8,000 psi. The pipe support system forces experience range form 40,000 lbf to more than 180,000 lbf depending upon location in the system. None of the mathematical methods used to arrive at these results are presented or discussed.

4.1.3 MODEL ANALYSIS RESULTS

The numerical results tell a story very different from that of the NRC post-accident analysis. There are two important results of the analysis. The first, and perhaps most significant result, involves the total fill time for the entire pipe. Figure 19 shows the condensate flow rates as a function of liquid fraction in the pipe, compared with the auxiliary feedwater flow rate into the system.

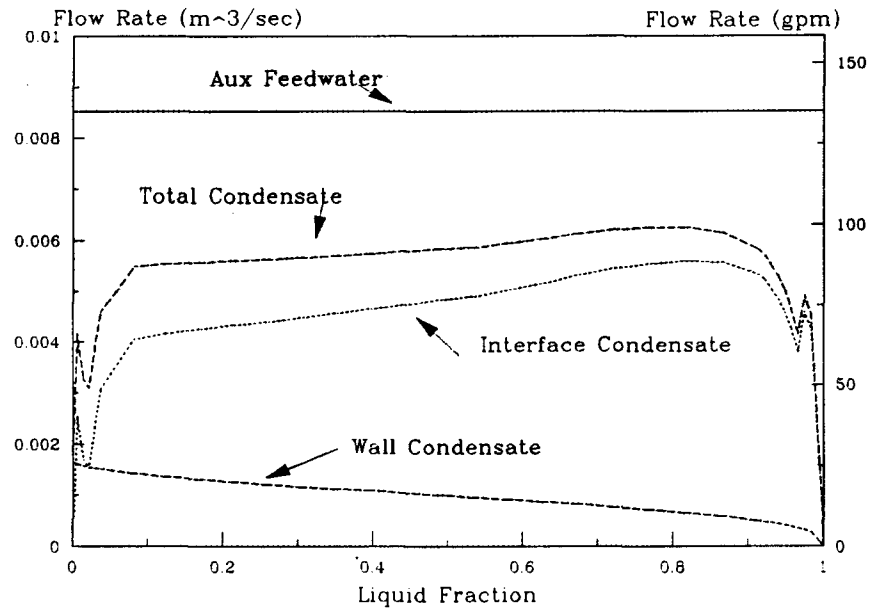

Figure (19): Condensate Volumetric Flow Rates

This figure shows that the input of saturated condensate is on the same order as the input of auxiliary feedwater flow rate into the system. When these condensate flow rates are figured into the calculation of the fill time for the pipe, we discover that the pipe becomes full of liquid after 3 minutes and 37.6 seconds of 135 gpm auxiliary feedwater input to the system. When one looks at this result in light of the known amount of time which elapsed, (12 min.), between start of auxiliary feedwater flow and the time that water-hammer occurred, it is clear that a steam void could not have been present in this section of the main feedwater line. Therefore, we must conclude that the water-hammer event took place in the feedwater nozzle of the steam generator and that the piping damage which

the main feedwater line experienced was the result of a pressure wave traveling from the feedwater nozzle to the auxiliary feedwater manifold.

The second important result of the numerical analysis comes from the interfacial stability model. Figure 20 shows the dimensionless axial distance from the subcooled liquid inlet where the interface instability begins as a function of dimensionless liquid depth.

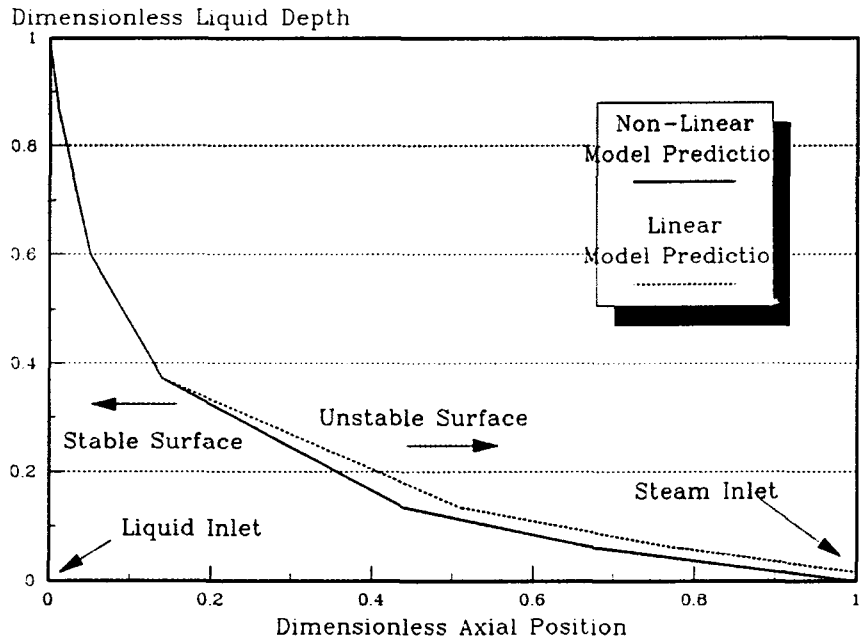

Figure (20): Surface Stability Transition Location

It can be seen that some part of the interface is unstable regardless of the liquid depth inside of the pipe. It also shows that the linear and non-linear instability models predict the same onset locations when the liquid depth approaches the top of the pipe. Because we know

that water-hammer did not take place during this time period of pipe fill up, that would seem to imply that there was no slug formation in the pipe during the fill up process. However, the stability model is predicting an increasing amount of surface area in the unstable mode as the liquid level in the pipe rises. So, how do we reconcile this contradiction? Two explanations are possible. The first would say that the interface stability models are wrong. Yet, these models have shown themselves to be in good agreement with prior experimental results. That leaves us with the second possibility. The prediction of interface stability is necessary, but not sufficient for predicting the collapse of a trapped steam pocket. This would imply that once bridging has occurred the slug itself may be stable or unstable. Hence, after bridging, the slug may break up before the trapped steam pocket is fully collapsed.

4.1.4 COMMENTS

As mentioned in section 4.1.2., the post-accident analysis of the NRC determined that the void fraction in the main feedwater line at the time of the water-hammer to be approximately 1-2 percent. A quick calculation of the volume of the main feedwater shows the line volume to be 3.123 cubic Meters, (825 gal.), based upon the pipe diameter of 0.253238 Meters and length of 62 Meters. Using the known auxiliary feedwater flow rates and their respective time of operation, we can calculate that, over

the 12 minute period between start of auxiliary feedwater and the water-hammer event, 3.379 cubic Meters, (892.5 gal.), of liquid was pumped into the main feedwater line. Base upon the auxiliary feedwater flow rates only, it could not be possible for the main feedwater line to have contained a steam pocket at the time of the water-hammer event. This simple calculation confirms the numerical analysis result that the main feedwater line had to be liquid solid at the time of the water-hammer event.

It is not clear how the NRC determined that the main feedwater line was partially voided by steam at the time of the water-hammer. Furthermore, it is not possible to analyze the feedwater nozzle for this case study due to a lack of plant physical geometry data on the steam generator feedwater ring. Therefore, we will move onto case study 2.

4.2 CASE 2: STEAM GENERATOR FEEDWATER NOZZLE FILLUP

In this case study, we will take a look at the problem of CIWH in the feedwater nozzle for a steam generator. In particular, the analysis will focus on the system which is present at the Trojan Nuclear Power Generating Station. The problem of CIWH in this section of the feedwater system is primarily the result of having the liquid level inside of the steam generator fall below the feedwater ring. This allows for the fluid inside of the feedwater ring to drain

out and be replaced by steam.

4.2.1 SYSTEM DESCRIPTION

Figure 21 shows the problem encountered when the steam generator liquid level drops below the feedwater ring level.

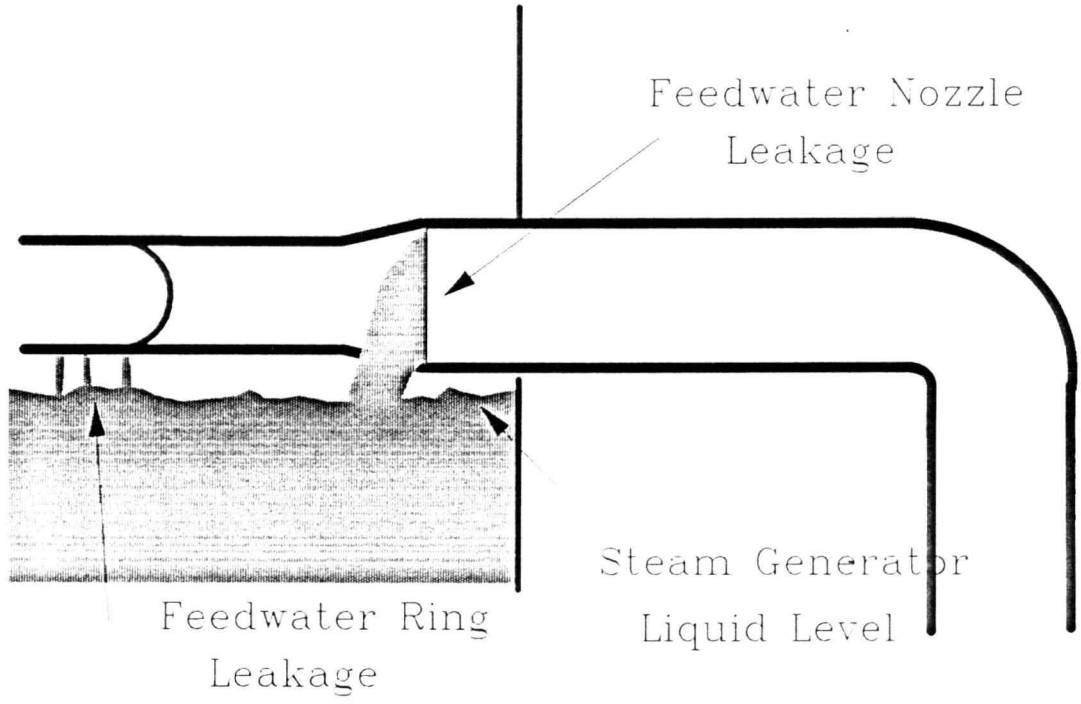

Figure (21): Steam Generator Feedwater System

The leakage of liquid from the feedwater nozzle is due to the gap in the connection between the feedwater ring and the nozzle section. This gap allows the feedwater system to drain and be replaced by steam. Water-hammer then becomes a concern during the refill of the feedwater ring and nozzle. The geometry and physical data for the system is taken from reference **[55]**. The feedwater nozzle diameter is 0.405 Meters and 1.2 Meters in length. The

feedwater ring diameter is 0.243 Meters and has an equivalent linear length of 23 Meters. The wall subcooling of the feedwater line outside of the steam generator is 26.5 Kelvin. The steam pressure is 6.21 MPa. The main feedwater temperature is 500 Kelvin.

4.2.2 ANALYSIS RESULTS BY FAILURE PREVENTION, INC.

The analysis by Failure Prevention, Inc., (FPI), is the result of a parametric study of feedwater flow rates into the feedwater ring and nozzle. The study uses the slug flow criterion of Baker, [1], and Wallis & Dobson, [22], to calculate the onset of slug formation and the resultant pipe system over-pressure and impact forces to non-compliant surfaces. The analysis by FPI concludes that slug formation, and thus water-hammer, will occur for any feedwater flow rate into the system.

The analysis is carried out for two different feedwater nozzle leakage rates. These flow rates are shown in Figure (22):. One for the current time of operation, and the second for end of plant life operation. These different feedwater nozzle leakages are due to the increase in the size of the gap at the ring-nozzle joint. The gap increase is the result of corrosion and erosion of the metal over the plant operation lifetime. The current gap width is 1.3 millimeters and the end of life gap width is estimated to be 3.3 millimeters.

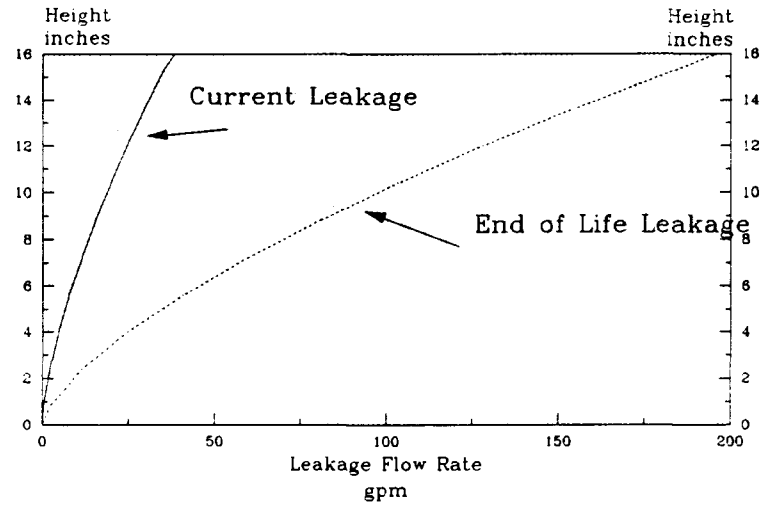

Figure 22 Nozzle Leakage Flow Rates

The report then calculates the maximum allowable fatigue strength for the most vulnerable pipe system support strut to be 188,000 lbf. The report also calculates the maximum water-hammer impact force as a function of feedwater flow rate. This analysis reveals that the maximum allowable feedwater flow rate to the system should be 50 gpm for 1991, and increasing linearly to 200 gpm at the end of plant life in 2020. Any flow rates greater than these will result in impact forces which exceed the allowable strut fatigue strength of 188,000 lbf.

4.2.3 MODEL ANALYSIS RESULTS

After running several different feedwater flow rate scenarios, the numerical analysis shows that there were no conditions which led to the onset of interface instability and subsequent bridging. This result immediately leads to the following question: How does water-hammer occur in this section of the feedwater system? The only obvious solution is as follows. Once the liquid level in the feedwater nozzle rises to the point where the feedwater ring is liquid solid, the only remaining source of steam to feed the condensation process inside of the system is through the gap at the feedwater ring-nozzle joint. Figure 23 shows the internal geometry of the feedwater nozzle.

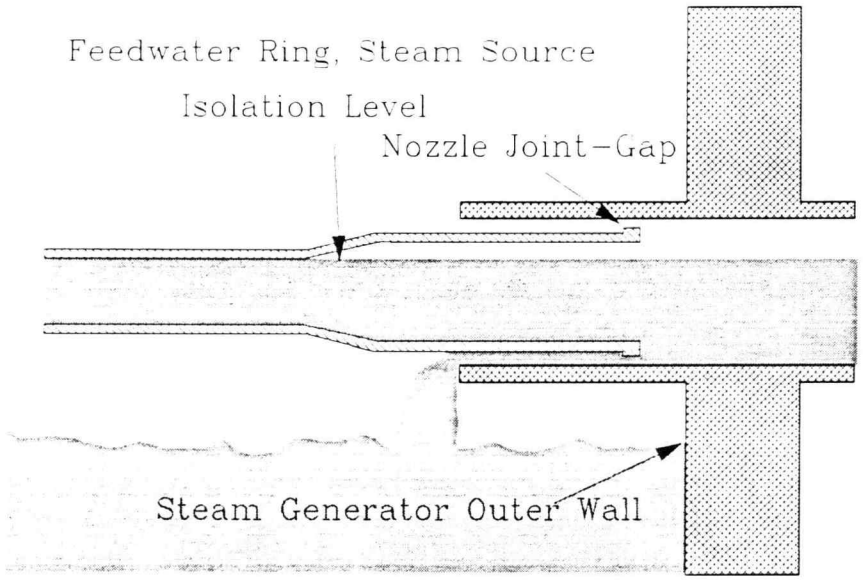

Figure (23): Feedwater Nozzle Joint-Gap Geometry.

Now the gap width, as stated in section 4.2.2., is small. Hence it is possible that the condensation rate inside of the system is greater than the rate at which steam can pass through the gap. Therefore, the remaining steam pocket in the feedwater nozzle is effectively isolated from its source. Thus, the liquid that is in the feedwater ring acts as a water slug and is driven back into the feedwater nozzle section.

If we use the above scenario as the basis for determining the water-hammer impact forces, it will be necessary to determine the interface temperature profile. By doing this, we can determine the minimum interface temperature. Once the minimum temperature is determined, it can be set equal to the minimum saturation temperature of steam which can remain in contact with the liquid interface and still condense. This minimum saturation temperature can than be used to establish the saturation pressure. This pressure value is then considered to be the lowest pressure possible in the collapsing steam pocket, and can be used in the calculation of the water-hammer over-pressure to which the piping system will be exposed.

The methods used to calculate the system over-pressure and impact forces are fully documented in NUREG/CR-5220, Vol. 1, **[56]**. Figure 24 shows the system over-pressure as a function of gross auxiliary feedwater flow rates.

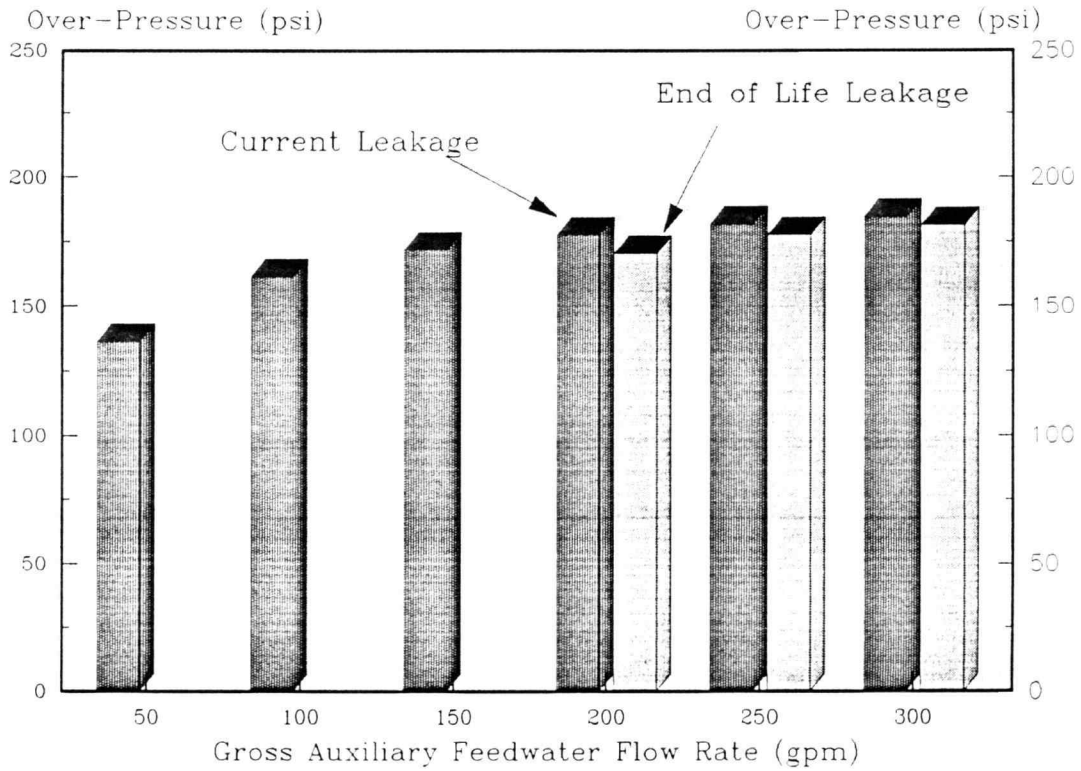

Figure (24): Feedwater Nozzle Over-Pressure

These over-pressure results are used to determine impact forces on main feedwater line non-compliant surfaces. Figure 25 shows the impact force as a function of gross auxiliary feedwater flow rates.

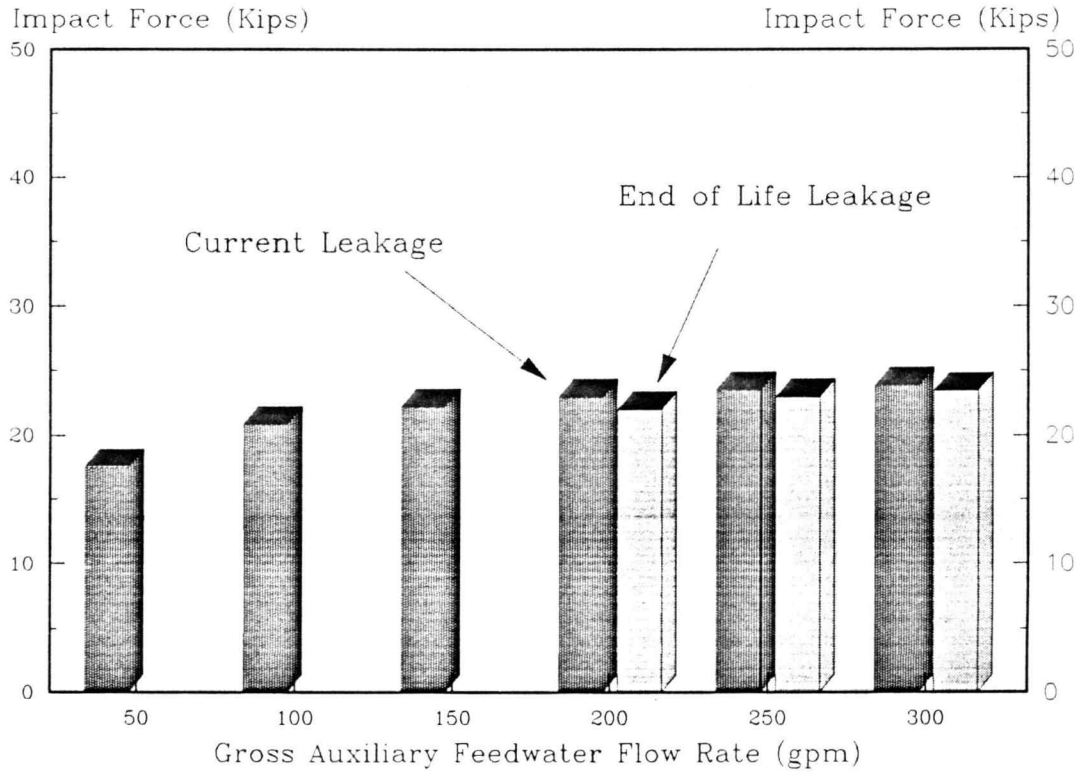

Figure (25): Main Feedwater System Impact Forces

These results are in good agreement with maximum allowable strut fatigue strength calculations by FPI. The numerical analysis is in agreement with the FPI results which use 50 gpm feedwater flow rate for the current operations maximum and the use of 200 gpm feedwater flow rate for the end of plant life operations.

4.2.4 COMMENTS

The maximum allowable strut fatigue strength calculated by FPI is based upon the assumption that every time there is a reactor trip, with its associated loss of main feedwater, that the liquid level in the steam generator is below the feedwater ring. This also assumes that there

will always be a water-hammer associated with each reactor trip. Neither of these assumptions are necessarily true. As a result, the actual maximum allowable strut fatigue strength could be much higher, thereby allowing the usage of higher feedwater flow rates.

There exists some uncertainty about the water-hammer scenario used in the numerical analysis. It is not clear that the current gap width is small enough to effectively isolate the steam pocket in the feedwater nozzle. It is also unclear that the gap width will be small enough at the end of plant life to isolate the steam pocket. If the gap width is not sufficiently small to isolate the steam pocket, then at some future point in time, it may not be possible to have any water-hammer events in the feedwater nozzle section.

5 SUMMATION

In this section we will review the thesis assumptions and numerical model results. Also, we will present some ideas for future work on this subject and suggestions for future model improvements. Finally, thesis conclusions will be presented.

5.1 ASSUMPTIONS & MODEL WEAKNESS

A short list of the important model assumptions and weaknesses is given as follows:

1. Flow of steam in the system is one dimensional.

2. Heat transfer surface areas are smooth.

3. Wave velocity is equal to inlet steam velocity.

4. All waves are absorbed at the terminal boundary.

5. Wave frequency and amplitude correlations are based upon very small data set.

6. Pipe wall heat transfer is one dimensional radially.

7. Auxiliary feedwater is dispersed uniformly in

system.

8. Condensate and system liquid are uniformly mixed.

9. Pressure drop and heat transfer correlations on the interface are highly dependent on wave amplitude correlation.

10. Spreadsheet code is large and very slow to run.

11. The built in assumptions about the applicability of the friction factor and heat transfer correlations needs to be considered before blindly using this code for analysis purposes.

5.2 REVIEW OF RESULTS

The numerical results presented in section 4 reveal the following:

1. For the pipe fillup in case study 1, it has been shown that the pipe had to be liquid solid at the time of the water-hammer event.

2. The bridging model predicts some surface instability over the entire duration of pipe fillup in case

study 1. This result implies that steam pocket collapse is not guarantied by the onset of bridging alone.

3. The bridging model does not predict surface instability for case study 2. This result implies that a void collapse mechanism other than slug formation on an unstable interface is at work.

4. The void collapse mechanism described in section 4.2.3 results in good agreement with the allowable strut fatigue strength impact force limits derived by FPI.

5.3 FUTURE WORK

The results of this thesis indicate that additional work needs to be done in order to more accurately describe the CIWH phenomenon. The most important thing which needs attention is the ability to accurately describe the phase interface wave structure. In particular, the determination of wave number, wave amplitude, and wave velocity under a variety of flow conditions.

The next item of work should be to use the more accurate interface structure models to make better estimates of the actual interface surface area. In this way, we would be able to use the more well known heat transfer coefficients for

smooth interface heat transfer while the interface turbulence would be accounted for by the increased surface area magnitudes.

Additional work is needed in the areas of slug dynamics. Specifically, slug stability and slug acceleration - steam void collapse. Future modeling of interfacial wave dynamics should take into account viscous wave damping, wave reflection off of the pipe walls, as well as constructive and destructive wave interference.

Finally, the development of a more accurate, multidimensional fluid-condensate mixing model is needed. This would allow for non-linear dispersion of auxiliary feedwater into the piping system, which would, in turn, improve the estimation of the interfacial temperature profile. The further addition of a model for circumferential conduction of condensate latent heat of vaporization in the pipe walls should also be included.

5.4 CONCLUSIONS

In presenting the conclusions to this thesis, it is important to keep in mind the statements of section 5.1. It is not intended that the results of the two specific case studies reviewed here be taken as universal truths about all horizontal piping systems. These conclusion should, however,

be seen as an indicator of the complexity of the phenomenon being studied, and a guide to further, more detailed analysis. The conclusions are enumerated as follows:

(1)-- The purpose of this study was to develop a method of estimating the potential for CIWH in a horizontal piping system. In order to accomplish this task, it was necessary to develop models for estimating the interfacial wave structure. This includes the correlations of frequency and amplitude data as functions of geometry and steam phase mass flow rate. The limited availability of data on this topic has made it very difficult to get an excellent statistical correlation.

(2)-- The computer model which was developed takes advantage of a newer, non-linear interface stability model to predict the onset of slug formation. The code also provides an estimate of the interfacial temperature, which is vital in determining the minimum possible pressure inside of a trapped steam pocket. Although the code itself does not contain over-pressure and impact force models, it does provide the necessary information to use in the methods published by the NRC.

(3)-- The code has helped to verify that the analysis of NUREG-1190, (Case Study 1), is incorrect in saying that the lower horizontal section of the main feedwater line was partially voided at the CIWH event time. This result has

shown that the CIWH had to have occurred in the steam generator feedwater nozzle assembly, and that the piping damage was due to the pressure wave which ensued. The code also reveals that the onset of slug formation is not sufficient to ensure that a trapped steam pocket will fully collapse.

(4)-- The code has helped in identifying a different CIWH mechanism in the steam generator, feedwater nozzle assembly, (Case Study 2). The code revealed no surface instabilities over the duration of the fillup transient. This result leaves open the possibility that CIWH can be eliminated from the feedring assembly by increasing the size of the nozzle joint-gap to ensure that the nozzle section cannot be isolated from the steam source. An experimental effort addressing this possibility could be performed. Finally, the thesis has identified areas which require more detailed analysis and better model refinement. It is hoped that these areas will be tackled in the future.

Bibliography

[1]Baker, O.; "Simultaneous Flow of Oil and Gas.", The Oil and Gas Journal, July 26, 1954, pages 185-195.

[2]Agrawal, S.S., Gregory, G.A., And Govier, G.W.; " An Analysis of Horizontal Stratified Two Phase Flow in Pipes. ", The Canadian Journal of Chemical Engineering, Vol. 51, June, 1973, pages 280-286.

[3]Mandhane, J.M., Gregory, G.A., and Aziz, K.; "A Flow Pattern Map for Gas-Liquid Flow in Horizontal Pipes.", International Journal of Multiphase Flow, Vol. 1, No. 4, 1974, pages 537-553.

[4]Spedding, P.L., and Van Thanh, N.; " Regime Maps for Air-Water Two Phase Flow. ", Chemical Engineering Science, Vol. 35, 1980, pages 779-793.

[5]Yoshihiro IIDA; "Prediction Method of Flow Patterns in Gas-liquid Two-phase Flow.", Bulletin of the JSME, Vol. 23, No. 176, February 1980, pages 247-254.

[6]Barnea, D., Shoham, O., Taitel, Y., and Dukler, A.E.; "Flow Pattern Transition For Gas-Liquid Flow In Horizontal And Inclined Pipes.", International Journal of Multiphase Flow, Vol. 6, 1980, pages 217-225.

[7]Shoham, O., and Taitel, Y.; "Stratified Turbulent-Turbulent Gas-Liquid Flow in Horizontal and Inclined Pipes.", AIChE Journal, Vol. 30, No. 3, May, 1984, pages 377-385.

[8]Barnea, D.; "A Unified Model For Predicting Flow-Pattern Transitions For The Whole Range Of Pipe Inclinations.", International Journal of Multiphase Flow, Vol. 13, No. 1, 1987, pages 1-12.

[9]Tandon, T.N., Varma, H.K., and Gupta, C.P.; "A New Flow Regimes Map for Condensation Inside Horizontal Tubes.", Journal of Heat Transfer, Vol. 104, November 1982, pages 763-768.

[10]Matuszkiewicz, A., Flamand, J.C., and Boure, J.A.; "The Bubble-Slug Flow Pattern Transition and Instabilities of Void Fraction Waves.", International Journal of Multiphase Flow, Vol. 13, No. 2, 1987, pages 199-217.

[11]Lin, P.Y., and Hanratty, T.J.; "Effect of Pipe Diameter on Flow Patterns for Air-Water Flow in Horizontal Pipes.", International Journal of Multiphase Flow., Vol. 13, No. 4, 1987, pages 549-563.

[12]Andritsos, N., And Hanratty, T.J.; "Interfacial Instabilities for Horizontal Gas-Liquid Flows in Pipelines.", International Journal of Multiphase Flow, Vol. 13, No. 5, 1987, pages 583-603.

[13]Helmholtz, H.; "Uber discontinuirliche Flussigkeitsbewegungen.", Wissenschaftliche Abhandlungen, 1882, pages 146-157.

[14]Lord Kelvin; "Hydrokinetic Solutions and Observations.", "On The Motion of Free Solids Through a Liquid.", and "Influence of Wind and Capillarity on Waves in Water Supposed Frictionless.", Mathematical and Physical Papers, iv, Hydrodynamics and General Dynamics, Cambridge, England, 1910, pages 69-85.

[15]Chandrasekhar, S.; "Hydrodynamic and Hydromagnetic Stability.", Oxford University Press, 1961, pages 481-514.

[16]Kordyban, E.S., and Ranov, T.; "Mechanism of Slug Formation in Horizontal Two-Phase Flow.", Journal of Basic Engineering, December 1970, pages 857-864.

[17]Taitel, Y., and Dukler, A.E.; "A Model for Predicting Flow Regime Transitions in Horizontal and Near Horizontal Gas-Liquid Flow.", AIChE Journal, Vol. 22, No. 1, 1976, pages 47-55.

[18]Mishima, K., and Ishii, M.; "Theoretical Prediction of Onset of Horizontal Slug Flow.", Journal of Fluids Engineering, Vol. 102, December 1980, pages 441-445.

[19]Hihara, E., and Saito, T.; "Slug Flow Transition in Horizontal Gas-Liquid Flow.", Bulletin of JSME, Vol. 27, No. 234, 1984, pages 2771-2778.

[20]Lin, P.Y., and Hanratty, T.J.; "Prediction of the Initiation of Slugs With Linear Stability Theory.", International Journal of Multiphase Flow, Vol. 12, No. 1, 1986, pages 79-98.

[21]Ahmed, R., and Banerjee, S.; "Finite Amplitude Waves in Stratified Two-Phase Flow: Transition to Slug Flow.", AIChE Journal, Vol. 31, No. 9, September 1985, pages 1480-1487.

[22]Wallis, G.B., and Dobson, J.E.; "The Onset of Slugging in Horizontal Stratified Air-Water Flow.", International Journal of Multiphase Flow, Vol. 1, 1973, pages 173-193.

[23]Gardner, G.C.; "Onset of Slugging in Horizontal Ducts.", International Journal of Multiphase Flow, Vol. 5, 1979, pages 201-209.

[24]Kubie, J.; "The Presence of Slug Flow in Horizontal Two-Phase Flow.", International Journal of Multiphase Flow, Vol. 5, 1979, pages 327-339.

[25]Johnston, A.J.; "Transition From Stratified to Slug Regime in Countercurrent Flow.", International Journal of Multiphase Flow, Vol. 11, No. 1, 1985, pages 31-41.

[26]Jepson, W.P.; "Modelling the Transition to Slug Flow in Horizontal Conduit.", The Canadian Journal of Chemical Engineering, Vol. 67, October 1989, pages 731-740.

[27]Lockhart, R.W., and Martinelli, R.C.; "Proposed Correlation of Data for Isothermal Two-Phase, Two-Component Flow in Pipes.", Chem. Eng. Prog., 1949, pages 39-45.

[28]Kadambi, V.; "Void Fraction and Pressure Drop in Two-Phase Stratified Flow.", The Canadian Journal of Chemical Engineering, Vol. 59, October 1981, pages 584-589.

[29]Johnston, A.J.; "An Investigation Into the Interfacial Shear Stress Contribution in Two-Phase Stratified Flow.", International Journal of Multiphase Flow, Vol. 10, No. 3, 1984, pages 371-383.

[30]Ainai, Y.L.; "An Extended Charnock Estimate of Interfacial Stress in Stratified Two-Phase Flows.", International Journal of Multiphase Flow, Vol. 12, No. 5, 1986, pages 839-844.

[31]Andritsos, N., and Hanratty, T.J.; "Influence of Interfacial Waves in Stratified Gas-Liquid Flows.", AIChE Journal, Vol. 33, No. 3, 1987, pages 444-454.

[32]Hagiwata, Y., Esmaeilzadeh, E., Tsutsui, H., and Suzuki, K.; "Simultaneous Measurement of Liquid Film Thickness, Wall Shear Stress and Gas Flow Turbulence of Horizontal Wavy Two-Phase Flow.", International Journal of Multiphase Flow, Vol. 15, No. 3, 1989, pages 421-431.

[33]Hart, J., Hamersma, P.J., and Fortuin, J.M.H.; "Correlations Predicting Frictional Pressure Drop and Liquid Holdup During Horizontal Gas-Liqiud Pipe Flow With a Small Liquid Holdup.", International Journal of Multiphase Flow, Vol. 15, No. 6, 1989, pages 947-964.

[34]Kim, H.J.; "Local Properties of Countercurrent Stratified Steam-Water Flow.", NUREG/CR-4417, October 1985, pages 76-111.

[35]Nusselt, W.; "Die Oberflachenkandensation des Wasser Dampfes.", Z. Ver. dt, Ing., Vol. 60, 1916, pages 541-575.

[36]Butterworth, D.; "An Analysis of Film Flow and its Application to Condensation in a Horizontal Tube.", International Journal of Multiphase Flow, Vol. 1, 1974, pages 671-682.

[37]Rifert, V.G.; "Heat Transfer and Flow Modes of Phases in Laminar Film Vapour Condensation Inside a Horizontal Tube.", International Journal of Heat and Mass Transfer, Vol. 31, No. 3, 1988, pages 517-523.

[38]Maron, D.M., And Sideman, S.; "Condensation Inside Near Horizontal Tubes in Cocurrent and Countercurrent Flow.", International Journal of Heat and Mass Transfer, Vol. 25, No. 9, 1982, pages 1439-1444.

[39]Chen, I.Y., and Kocamustafaogullari, G.; "Condensation Heat Transfer Studies for Stratified, Cocurrent Two-Phase Flow in Horizontal Tubes.", International Journal of Heat and Mass Transfer, Vol. 30, No. 6, 1987, pages 1133-1148.

[40]Thomas, R.M.; "Condensation of Steam on Water in Turbulent Motion.", International Journal of Multiphase Flow, Vol. 5, 1979, pages 1-15.

[41]Theofanous, T.G., Houze, R.N., and Brumfield, L.K.; "Turbulent Mass Transfer at Free, Gas-Liquid Interfaces, With Applications to Open-Channel, Bubble and Jet Flows.", International Journal of Heat and Mass Transfer, Vol. 19, 1976, pages 613-624.

[42]Celata, G.P., Cumo, M., Farello, G.E., and Focardi, G.; "A Theoretical Model of Direct Contact Condensation on a Horizontal Surface.", International Journal of Heat and Mass Transfer, Vol. 30, No. 3, 1987, pages 459-467.

[43]Celata, G.P., Cumo, M., Farello, G.E., And Focardi, G.; "Direct Contact Condensation of Steam on a Horizontal Surface of Water.", Warme- und Stoffubertragung, Vol. 21, 1987, pages 169-180.

[44]Celata, G.P., Cumo, M., Farello, G.E., And Focardi, G.; "Direct Contact Condensation of Steam on Slowly Moving Water.", Nuclear Engineering and Design, Vol. 96, 1986, pages 21-31.

[45]Celata, G.P., Cumo, M., Farello, G.E., and Focardi, G.; "A Comprehensive Analysis of Direct Contact Condensation of Saturated Steam on Subcooled Liquid Jets.", International Journal of Heat and Mass Transfer, Vol. 22, No. 4, 1989, pages 639-654.

[46]Celata, G.P., Cumo, M., Farello, G.E., And Focardi, G.; "Direct Contact Condensation of Superheated Steam on Water.", International Journal of Heat and Mass Transfer, Vol. 30, No. 3, 1987, pages 449-458.

[47]Segev, A., Flanigan, L.J., Kurth, R.E., and Collier, R.P.; "Experimental Study of Countercurrent Steam Condensation.", Journal of Heat Transfer, Vol. 103, May 1981, pages 307-311.

[48]Lim, I.S., Tankin, R.S., and Yuen, M.C.; "Condensation Measurement of Horizontal Cocurrent Steam/Water Flow.", Journal of Heat Transfer, Vol. 106, May 1984, pages 425-432.

[49]Kim, H.J., and Bankoff, S.G.; "Local Heat Transfer Coefficients for Condensation in Stratified Countercurrent Steam-Water Flows.", Journal of Heat Transfer, Vol. 105, November 1983, pages 706-712.

[50]Jung-Hoon, C., Shimko, M.A., And Sonin, A.A.; "Vapor Condensation onto a Turbulent Liquid--I. The Steady Condensation Rate as a Function of Liquid Side Turbulence.", International Journal of Heat and Mass Transfer, Vol. 29, No. 6, 1986, pages 1319-1332.

[51]Jung-Hoon, C., Shimko, M.A., and Sonin, A.A.; "Vapor Condensation onto a Turbulent Liquid--I. Condensation Burst Instability at High Turbulence Intensities.", International Journal of Heat and Mass Transfer, Vol. 29, No. 6, 1986, pages 1333-1338.

[52]Welty, J.R., Wicks, C.E., And Wilson, R.E.; "Fundamentals of Momentum, Heat, and Mass Transfer.", John Wiley & Son's, 3rd Edition, 1984, pages 154-156.

[53]Lotus Development Corporation, 55 Cambridge Parkway, Cambridge, MA 02142, 1987, Version 2.0.

[54]NUREG-1190, San Onofre Accident Analysis, 1986.

[55]Failure Prevention, Inc.; "Auxiliary Feedwater Flow Requirements for Water Hammer Prevention at the Trojan Nuclear Plant.", PGE contract report, No. 87-015, December 2, 1987.

[56]NUREG/CR-5220, Creare TM-1189, Vol. 1 & 2, 1988.